AC

D4992649

SAND79-7099
Unlimited Release
UC-94b

Development of Cellulose Flywheel Rotors Final Report

Arthur G. Erdman, David L. Hagen, Darrell A. Frohrib

Prepared by Sandia Laboratories, Albuquerque, New Mexico 87185
and Livermore, California 94550 for the United States Department
of Energy under Contract DE-AC04-76DP00789

Printed February 1980

Sandia National Laboratories

SF 2900-Q(3-80)

Issued by Sandia Laboratories, operated for the United States Department of Energy by Sandia Corporation.

Printed in the United States of America

Available from
National Technical Information Service
U. S. Department of Commerce
5285 Port Royal Road
Springfield, VA 22161

Price: Printed Copy $6.00 ; Microfiche $3.00

SAND79-7099
Unlimited Release
Printed March 1980

Distribution
Category UC-94b

DEVELOPMENT OF CELLULOSE FLYWHEEL ROTORS

FINAL REPORT

Sandia Contract 07-9072

Prepared for

SANDIA LABORATORIES
Albuquerque, New Mexico 87185

Technical Contract Monitor
Harold E. Schildknecht, Division 2324

Prepared by

Arthur G. Erdman
David L. Hagen
Darrell A. Frohrib

Mechanical Engineering Department
University of Minnesota
Minneapolis, MN 55455

Report UMN-ME-FL-79-03

ABSTRACT

The primary tasks addressed were: I) The design and development of durable hub-to-rotor attachments and the balancing and vibrational analysis of the resulting hub-rotor systems. II) Measuring and analyzing the strength distributions and durabilities of different types of plywood and of hub-rotor systems. In accomplishing these tasks, a new metallic-hub to cellulosic-rotor bonding attachment was designed which utilizes a flexible scalloped metal-band in lieu of the traditional elastomeric layers to accommodate the differential strain between rotor and hub. With the objective of eliminating the need for adding or removing mass to balance rotors, a self-centering dynamic balancer was designed to automatically locate the inertial axis of a rotor. Attaching the hubs and shafts concentric and parallel with the inertial axis will accomplish the balancing of the rotor during assembly. In analyzing rotor vibrations, a nondimensional design parameter was derived which correlates the support flexibility required to the useable strength and length of the rotor for a useful operating range above the transverse critical frequency. The tensile strengths of conventional Finnish birch plywood were measured in three directions using material equilibrated at 50% relative humidity and vacuum-dried material. Similar measurements of custom-made, hexagonal, yellow birch plywood showed double the mid-ply strengths. The standard deviation of the measured strengths and the drop in mean strength with vacuum drying were both on the order of 10%. High resolution (0.01%) microprocessor data acquisition equipment was assembled to monitor tensile tests. Digital circuitry was designed to monitor the acoustic emission energy with 65 dB S/N ratio. Cyclic tensile fatigue test equipment was modified for the fatigue testing of plywood samples. A dynamic cyclic fatigue apparatus

capable of simultaneously driving two rotors in separate vacuum containers at 10 kW was designed. A pseudodynamic hub-rotor fatigue tester was designed and built from existing flexural fatigue testing apparatus.

TABLE OF CONTENTS

List of Illustrations

List of Tables:

SUMMARY

This program focused on the assembly factors and design parameters required to develop low cost flywheel energy storage systems utilizing cellulosic materials. The primary tasks addressed were:

I. The design and development of durable hub-to-rotor attachments and the balancing and vibrational analysis of the resulting hub-rotor systems.

II. Measuring and analyzing the strength distributions and durabilities of different types of plywoods and of hub-rotor systems.

The activities and accomplishments during this program are summarized as follows:

A new design for a hub-to-rotor interface was developed which basically consists of a flexible scalloped metal band mounted on the stepped end of a plywood rotor. By appropriately stepping the rotor ends with plywood disks of different diameters, it is possible to approximate a constant stress rotor with a minimum of material wastage. A scalloped flexible metal-band wrapped around and bonded to both the hub and last (outermost) disk provides a durable hub-to-rotor attachment configuration. This configuration is rigid in torque and axial moment, while still providing the radial flexibility required to accommodate the differential strain between the cellulose rotor and the metal hub.

Alignment methods of balancing rotors were examined which offer the potential for replacing the conventional mass removal-or-addition methods. Toward this end, a self-centering dynamic balancer was designed to automatically locate the inertial axis of the rotor and to facilitate the attachment of the hubs and shafts parallel and concentric to that axis while the rotor is spinning. The objective is to enable any rotor with a

pseudoisotropic core to be balanced directly as it is assembled.

The fundamental transverse vibrations of a rotor were analyzed parametrically as functions of the material properties and rotor dimensions. A nondimensional design parameter was derived which directly correlates the flexibility required in the rotor supports to the length and useable strength of the rotor for a useful operating range above the fundamental transverse critical frequency. The transmissibility of an experimental rotor and support system was measured as a function of frequency, and the critical transverse frequency located.

A series of tensile tests and density measurements were conducted to evaluate the design intrinsic specific energy (the ratio of tensile strength to density) of commercially available birch plywood. This conventional crossply material exhibited a fairly broad distribution of strengths with the standard deviations ranging from 12% to 20%. Vacuum-drying plywood that had previously been equilibrated at 50% relative humidity, resulted in a decrease in tensile strengths ranging from 5% to 20% as had been anticipated from trends observed in related literature. The strength of vacuum-dried birch plywood at 45° to the plies was 30.5% of the average of the strengths in the parallel and perpendicular directions. Properties along this 45° direction to the plies (i.e., the direction which bisects the grain axes of the adjacent plies) are expected to correlate best with spin tests.

The hexagonal birch plywood (0°, 60°, -60°) utilized in the plywood evaluation program was custom-made in a commercial plywood factory. When equilibrated at 50% relative humidity, this material exhibited a specific intrinsic energy of 50 kJ/kg (6.3 Whr/lb) in its weakest axis--

the one that bisects adjacent plies. This value is double the corresponding value for the conventional crossply material; also, the weakest-axis vs. strongest-axis strength ratio for the hexagonal material is 88% higher than for the crossply. The hexagonal material exhibited a tighter frequency-distribution of tensile strength measurements than the crossply, but this may have been due to the use of clearer (fewer blemishes) veneers. In any event, for these two plywood types, the hexagonal material displays superior performance relative to flywheel-use potential, and this performance could be improved through better manufacturing control and appropriate nondestructive proof testing.

A microprocessor-based data acquisition system was assembled capable of monitoring the data at several thousand points a second with 0.01% resolution; furthermore, data can be averaged and then recorded at several hundred points a second. The results would most likely be numerically differentiated to examine the 1% nonlinearity that typically occurs. This system was essentially available for use at the completion of the present contract. In light of that availability, a follow-on program has been proposed for the performance of high resolution tensile testing to measure the nonlinearity of the tensile load-deformation curve and to attempt to correlate the change in elasticity with the long-term strength.

It is theorized that the acoustic energy released during tensile testing will correlate with the changes in the elasticity of the sample. Hence, ultrasonic sensors, amplifiers and analog recorders were acquired to monitor the acoustic emissions anticipated through 100 kHz. High speed digitizing (12 bit @ 500 kHz) and digital multiplication and accumulation electronics were designed and the parts ordered so that the acoustic

emission signal could be accurately acquired and then squared and integrated to give a gross 65 dB signal-to-noise (S/N) ratio in the resulting accumulated acoustic emission energy. The energy in the acoustic emissions thus acquired can be digitally recorded along with the load-deformation data, and the results numerically correlated. This acoustic emissions test system was still undergoing development at the completion of the present contract. However, it is believed to hold promise for advancing the state of the art of acoustic emission analysis for plywood and other materials.

A cyclic eccentrically-driven tensile-fatigue machine was modified for plywood tensile samples, and an environmental box built to contain it. However, calibration studies revealed that the low stiffness of the plywood samples lowered the resonance point of the machine significantly below its design operating point, the latter having been established for use with metals. Transmissibilities significantly greater than unity were found, indicating that the stress cycle depended on the sample stiffness. Since this varies among samples as well as during the fatigue test, the equipment could not be effectively calibrated in the present mode of operation. Future usability of the machine is conditional on installing a load cell to monitor the stresses actually experienced during the test program.

A cyclic rotary fatigue test apparatus was proposed early in the program to test two rotors simultaneously under actual operating conditions. Detailed designs were made for such an apparatus which would be capable of testing rotors up to 1.5 m (5 ft) in diameter at a power level of 10 kW (13 hp) over a speed range of 1800 to 5500 rpm. However, the cost and effort required for the project proved to be beyond the resources available. The rotor fatigue-testing task was therefore modified to test experimental

hub-to-rotor attachments in moment and torque simultaneously, in a pseudo-dynamic situation. An existing bending fatigue machine was modified to perform this testing and is available for use in future programs. The cyclic rotary fatigue testing concept is worthy of consideration for use in any future programs that would involve the testing of fully assembled rotors in late stages of design.

It is anticipated that the drying rates of cellulosic materials in a vacuum will significantly affect the technical and economic feasibility of using such materials in flywheel rotors. Hence, preliminary experiments were made to evaluate the diffusion coefficients for plywood rotors. The validity of the equations used and the appropriate parameters for vacuum drying will need to be examined further in future studies.

INTRODUCTION

Solar energy systems require energy storage to buffer the variable demand and the fluctuating availability of solar insolation and of wind. High efficiencies, durability, and low costs are very important in making such energy storage systems economical to the public. Flywheel energy storage systems have the potential for such energy storage applications if they can be made cost effective. Efforts have therefore been made to improve the performance and reduce the costs of flywheel energy storage systems.

A. BACKGROUND

The rotor represents a major fraction of the cost of the system. In 1972, cellulosic materials were recognized by D. W. Rabenhorst at the Applied Physics Lab, as potential candidates for low cost flywheel rotors. (1) Later reviews by the present authors showed that these cellulosic materials still looked promising, so a preliminary research program was initiated to develop and test flywheel systems using cellulosic rotors. (2,3) Spin tests of plywood disks by Rabenhorst demonstrated preliminary technical feasibility. (4) Tapered birch plywood disks were used as convenient cores around which higher performance materials such as Kevlar, fiberglass and steel hose-wire were wound.

Further work was done at the University of Minnesota on developing plywood rotors and in conducting preliminary studies of the material properties of plywood for such rotors. (5) In addition studies of the supports, dynamics, and controls were begun. A model flywheel demonstration-system was built using a plywood rotor. Later, a detailed study was made of the economics of assembling cellulosic rotors for the Applied Physics Lab. (6) This indicated that plywood rotors were marginally competitive with E-glass or steel hose-wire rotors, primarily due to comparatively higher container costs. However,

of all the materials examined, the so-called "superpaper" made by highly orienting fibers during manufacture potentially provides the rotor with the lowest energy storage costs. Further studies were made of the sensitivity of flywheel system economics to using cellulosic cores or rotors, and to the container costs. (7) Plywood or similar pseudoisotropic materials definitely appear to be useful materials to make cores around which to wrap E-glass or steel hose-wire while economically contributing to the energy storage potential of the rotor. (8) "Superpaper" rotors appear even more competitive at lower container costs.

To commercialize such cellulosic rotors, their technical feasibility must be demonstrated. Reliable methods of designing, assembling and balancing plywood and paper rotors must be developed. The strength and durability of cellulosic materials under vacuum conditions must also be measured before they can be designed into this high performance application. These material properties control the energy storage capabilities of the rotors, and the resulting storage economics.

B. CURRENT PROJECT

To demonstrate the technical feasibility of cellulosic rotors, a proposal was made to the Department of Energy to study these areas as part of the overall Solar Mechanical Energy Storage Project work administered by Sandia Laboratories. Two primary tasks were addressed in this proposal:

I. The design and development of durable hub-to-rotor attachments and the balancing and vibrational analysis of the resulting rotor.

II. Measurements of the strength distribution and durability of plywood and the hub-rotor system.

These technical factors are critical to the commercial feasibility of cellulosic rotors.

A contract was received from Sandia Laboratories in August 1978 for the duration of one year. A number of designs were developed, equipment built, and measurements taken in the course of performing the above mentioned tasks. The reasons for addressing the tasks, the methods and results in performing them, and the observations and conclusions that resulted are described in the following sections which are organized according to the primary tasks addressed.

I. HUB-ROTOR DEVELOPMENT AND BALANCING METHODS

The primary rotor configurations of interest (see Figure 1) are the purely cellulosic rotor such as a plywood cylinder, a compound rotor wound around a plywood core, or a wound rotor of superpaper (such as the kraft-paper cylindrical rolls as they come off a paper mill). The plywood cylindrical-rotor is readily constructed using commercially available Birch plywood. This configuration was examined at the University of Minnesota as it appeared to be immediately marketable as cores for higher performance materials. It is recommended that subsequent studies examine conventional high performance kraft paper and develop methods to manufacture "superpaper".

A. HUB TO ROTOR ATTACHMENT

The main problem with bonding a flat, round, metallic hub to a cellulosic rotor is that the two materials have different Young's moduli. When spun up to operating speeds, the rotor expands much more than the hub causing a large differential strain and shear stress in the bonding layer which leads to failure of the bond or of the cellulose material. (4) (See Figure 2a). Three approaches are possible to eliminate this stress concentration and cause of rotor failure.

1. Shape the rotor to reduce the stresses and strain in the rotor at the hub interface.
2. Insert an elastomeric layer in between the rotor and hub to absorb the differential strain.
3. Change the configuration of the hub-to-rotor attachment.

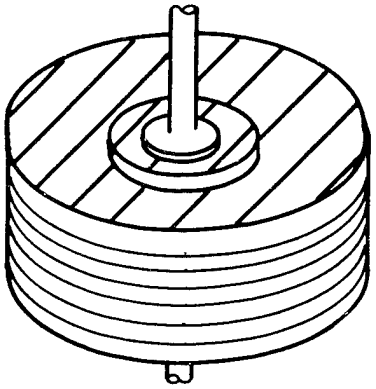

PSEUDOISOTROPIC
ROTORS OF PLYWOOD
OR FIBERBOARD DISKS

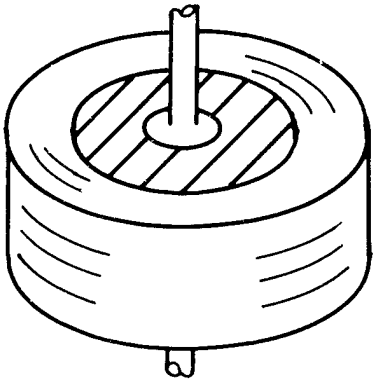

COMPOUND BARE FILAMENT
ROTORS OF STEEL HOSE
WIRE OR E-GLASS FILAMENT
WOUND AROUND A PLYWOOD
CORE

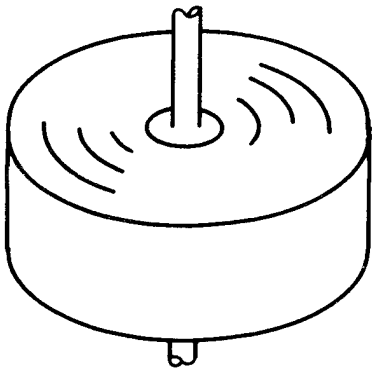

ROLLED PAPER ROTOR
SUPERPAPER MADE OF
HIGHLY ALIGNED FIBERS
PROMISES THE HIGHEST
PERFORMANCE/COST

Figure 1. Cellulosic Rotor Configurations

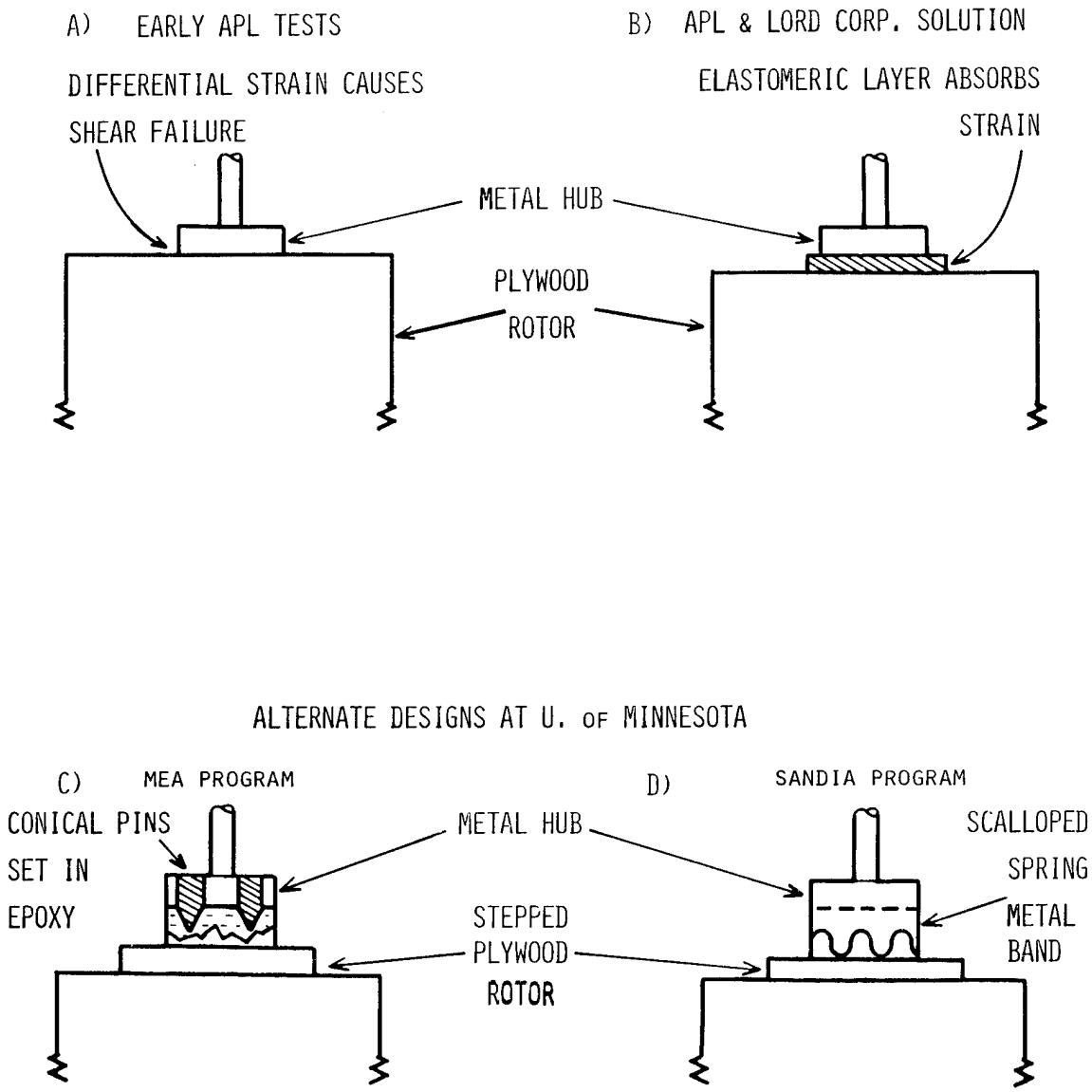

Figure 2. Hub-to-Rotor Attachments

These three approaches are discussed as follows:

1. Shape the Rotor

This first approach is aimed at reducing rotationally induced stresses in the rotor near the hub by shaping it, thus reducing the strain and the differential shear stress at the hub to rotor interface. Elaborate shaping of the rotor is used in satellite applications to obtain a constant stress throughout the rotor. Shaping pseudoisotropic materials however results in material waste and additional labor, compared to isotropic materials such as steel which can be cast in that shape. This would reduce the commercial competitiveness of the rotor. The cellulosic rotor economic study performed for the Applied Physics Laboratory revealed that in a first order analysis, a cylindrical rotor results in the lowest storage costs when considering the rotor and vacuum container costs. (6) (See Figure 3.)

A closer analysis shows that the vacuum containers required to minimize aerodynamic drag usually have their ends dished slightly outward which would allow room for some shaping near the rotor hubs without increasing the vacuum container cost. A rotor can be shaped to advantage by stepping its ends using appropriately sized disks. These disks can be economically made on an automatic ("pin") router by cutting them out to be different fractional diameters of the nominal diameter of the rotor (e.g., one-half, one-third, and one-quarter). These disks would then be bonded to the ends of the rotor using simple centering jigs made of a very hard rubber to provide uniform pressure. (See Figure 2 C & D and Figure 4.) The resulting form would approximate the hyperbolic shape of a constant stress isotropic rotor. There would be minimal material wastage in the finish contouring of the rotor due to the prior "stepping" of its ends, and little or no additional cost would be anticipated for the vacuum container to accommodate the rotor's hyperbolic shape. The optimal shape for a pseudoisotropic rotor, however, is not obvious since the radial strength is considerably higher

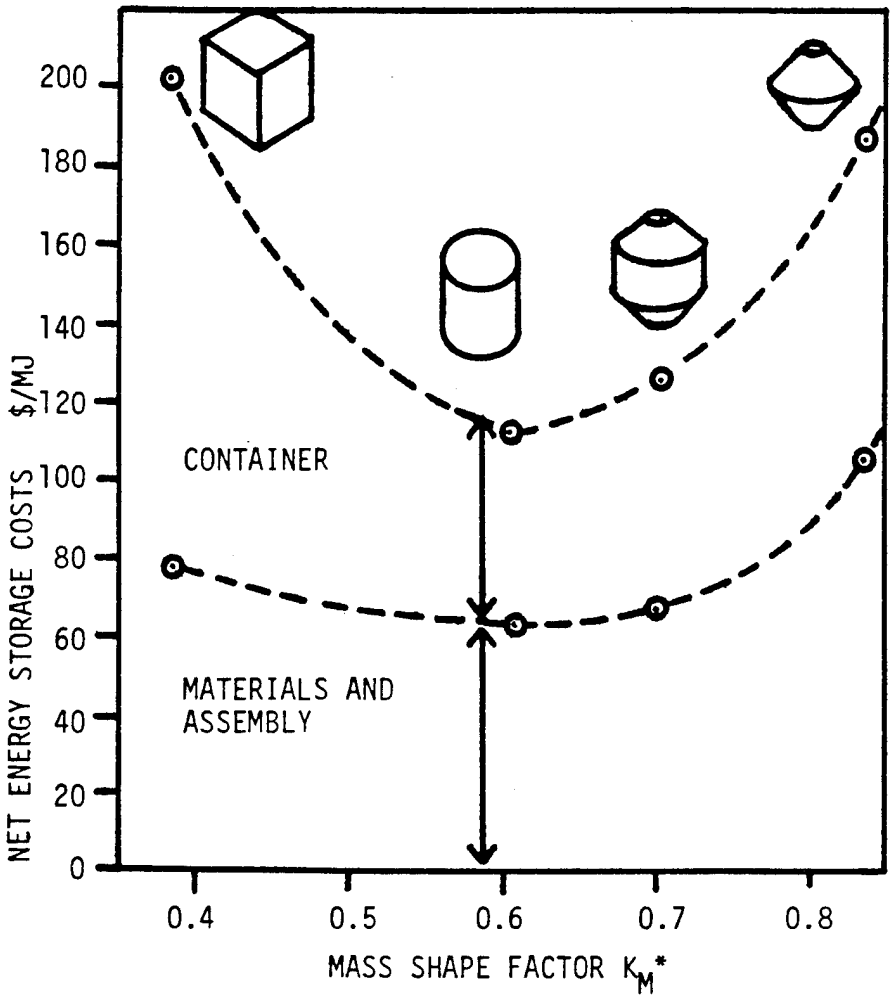

THE CURVES ASSUME CONSTRUCTION OF A PLYWOOD ROTOR WITH MATERIAL AND ASSEMBLY COSTS ASSUMED PROPORTIONAL TO THE MATERIAL UTILIZATION FACTOR. CONTAINER COSTS WERE ASSUMED TO BE $\$700/M^3$.

*K_M ACCOUNTS FOR THE NONUNIFORM STRESS DISTRIBUTION IN THE ROTOR DUE TO ITS SHAPE AND CONSTRUCTION; HENCE, IT IS A MEASURE (DIMENSIONLESS) OF HOW EFFICIENTLY THE STRENGTH OF THE ROTOR MATERIAL IS UTILIZED.

Figure 3. Effect of Rotor Shape on Storage Costs

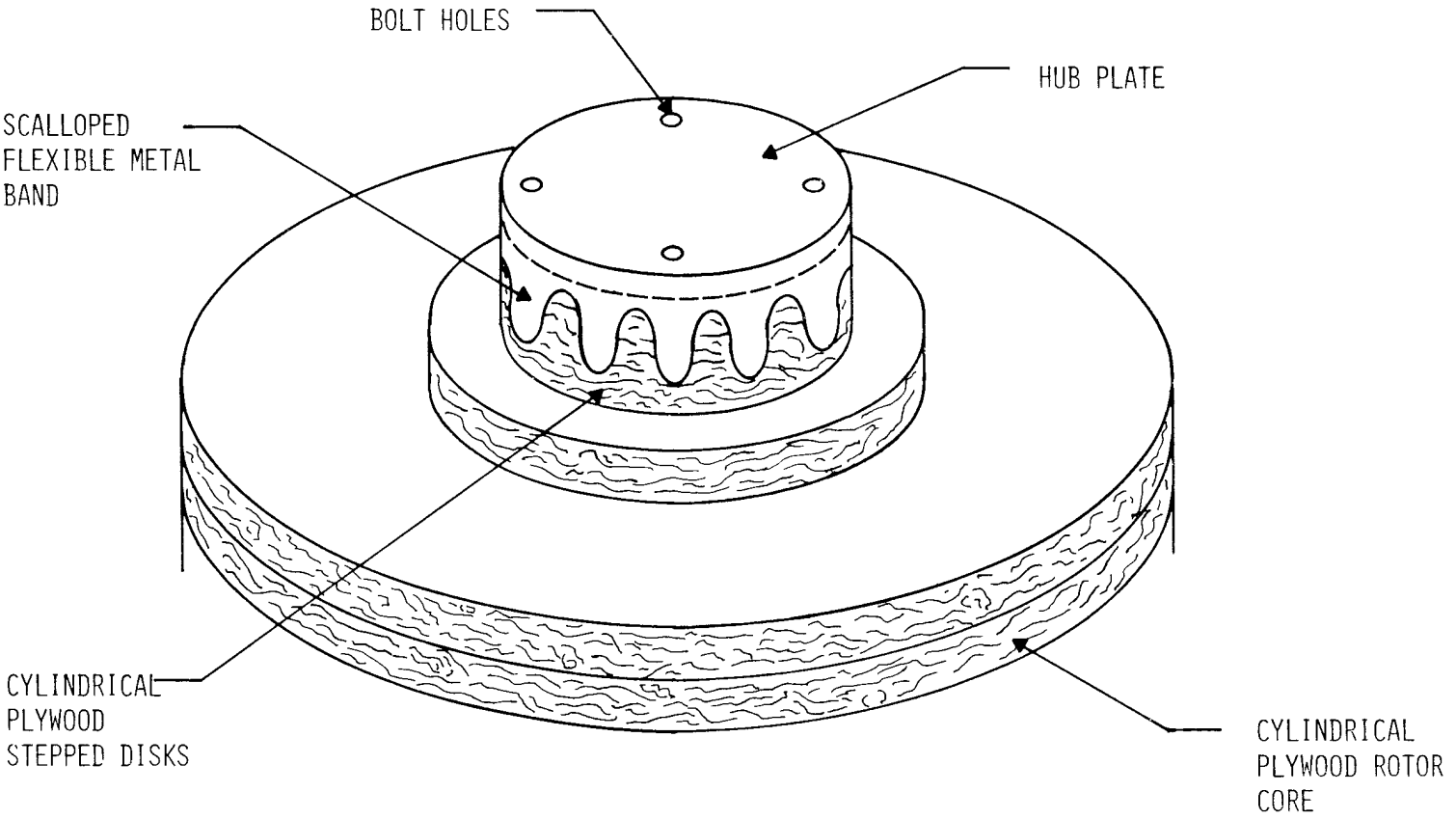

HUB ATTACHMENT IS RIGID IN APPLIED TORQUE AND IMBALANCE MOMENT BUT FLEXIBLE IN CENTRIFUGAL EXPANSION.

Figure 4. Flexible Band Hub-to-Rotor Attachment, University of Minnesota, 1979

than that axial strength. An ellipsoid may be a more suitable shape and this question requires further analysis utilizing the full orthotropic properties of the material layers and the adhesives used to bond them together.

2. Elastomeric Interface

The second approach of placing an elastomeric layer between the hub and rotor (see Figure 2B) was successfully developed by Rabenhorst of APL and McGuire of Lord Corporation.(4,8) The elastomeric layer is vulcanized in place between the hub and rotor. This bond has survived rotor failures and no longer appears to be a limiting factor in the short term. One difficulty in assembling such a hub attachment is the possibility of overheating the plywood or fiberboard in the process, causing the water present to turn to steam. If sufficient pressure is not applied, this will cause a "blister" or adhesive failure between the top plies. This can be avoided through careful control. However, moisture gradients and thermally induced stresses and possible material degradation are still potential problems due to the high heat. These could be partly eliminated by drying the plywood thoroughly beforehand.

An alternate method to this elastomeric approach is to cut a layer of elastomer from a sheet and bond it to the hub and rotor with adhesive (e.g., a contact adhesive such as "Plyobond"). This method was also found to be effective in eliminating hub to rotor failures in short-term burst tests. The long-term fatigue strength of both these bonding methods, however, would need to be proven (see Section IID). A further potential difficulty is the possibility that the added damping provided by the elastomeric layer would amplify the whirl-modes and resonances occurring in the rotor suspension system since they occur at the rotor rather than between the supports and ground.(9)

3. Alternate Hub Configurations

The third approach is to change the configuration of the hub-to-rotor attachment to minimize the stresses caused by the rotational expansion while still providing sufficient bonding to sustain the torque required to transmit power, and the bending moment and shear due to imbalance. One such approach was developed by our team in a separate development program with the Minnesota Energy Agency.(7) In that design, conical studs were used to bond the hub to the rotor in addition to using the stepped-rotor approach to minimize the strains involved. (See Figure 2C.) Cylindrical studs set in place with epoxy have been effectively developed for boats by the Gougeon Brothers of Bay City, Michigan. Such studs-to-wood bonds have been demonstrated to sustain 1500 psi in shear over their surface before failing.(10) The conical shape is hypothesized to distribute the strains more uniformly than a simply cylindrical stud. This design may be difficult to implement and expensive.

A simpler alternate design for such a different hub configuration was developed under this contract and is shown in Figure 2D. In this design, the hub plate is bonded to a cellulosic disk of the same size which is the last disk of the stepped rotor design. Then a metal band is wrapped around the hub and disk combination, and bonded to both. The part of the band extending over the cellulosic disk is cut (stamped) into tabs (see Figures 2D and 4). This will allow the band to flex radially outward by bending as the rotor is spun up since the cellulose disk expands faster than the metal hub. The band-to-disk bond would experience very little strain and stress in such flexure and should therefore remain intact throughout the life of the rotor. The metal band would need to flex very little, and if made of fatigue resistant metal such as spring steel, should experience no problems with failure.

While the band is flexible in radial expansion, it will still be circum-

ferentially rigid. It is therefore able to withstand the torque required to transmit energy to and from the rotor. The band-to-disk bond would also resist a moment and shear applied between the hub and rotor as would occur if the rotor were not perfectly balanced. There would also be little damping to amplify the whirl or critical resonance modes compared to the elastomeric pads.

The band is cut into tabs with circular, elliptical or sinusoidal shapes in the notches to minimize stress concentrations. This design can be modified to easily accommodate conical or similarly shaped rotors by bending the tabs to such a shape. This design thus appears to be applicable to flywheel rotors in general where a hub and rotor of dissimilar materials need to be connected together, i.e. it could be used for pseudoisotropic rotors of fiberglass or graphite, as well as for compound rotors of filaments wound around an isotropic or pseudoisotropic core.

In conclusion, the hub-to-rotor bond failure problem has previously been solved by introducing an elastomeric layer at the interface. In this present project, an alternate design was developed consisting of a stepped rotor made of disks of fractional sizes, and attached to the hub with a flexible scalloped metal-band. This design is seen as being cost competitive with the elastomeric layer approach and is expected to be more durable and provide greater rigidity between the hub and rotor than the latter. A prototype was not constructed due to limitations in time and funds.

B. BALANCING

If the geometric axis of rotation of a rotor does not coincide with one of its principle inertial axes, there will be an "imbalance" resulting in vibration, stress and fatigue in the rotor supports. Eliminating or minimizing this effect is of primary concern in the design and assembly of flywheel rotors. Conventional approaches to this problem use flexible rotor supports to minimize the stresses, and remove or add mass to the rotor to change its inertial axis so

that it coincides with the geometric axis. (See Figures 5A & B.) The corollary balancing method is to adjust the supports so that the inertial axis of the rotor is aligned with the geometric rotational axis. (See Figures 5C & D.) The latter is not commonly done, but appears preferable for high performance rotors, especially those using anisotropic materials. Hence, the balancing concept of dynamically locating the rotor's inertial axis and attaching the hubs and shafts in alignment with that axis while the rotor is spinning was conceived and developed as part of the work of this contract.

1. Rotor Modification and Alignment Methods

In conventional practice, rotors are balanced by removing mass by drilling holes in the periphery of the rotor (as in the flywheels in automotive engines) or by adding compensating weights to the rotor (as in automotive tires). Pseudoistropic rotors made of plywood or fiberboard could be conventionally balanced by removing weight around the periphery fairly readily (see Figure 5A). Drilling holes in the rotor would induce undesirable stress concentrations and premature failure. Therefore it is recommended that material be removed by sanding it off the outer periphery surface of the rotor in large thin patches of surface area.

For a compound wound rotor where high performance filaments of fiberglass or steel wire are wound around a cellulosic core, such a material removal process does not appear practical. It may still be possible to add weights to the inner rim of the rotor. However there is the danger that the weights could work loose during the flywheel's operation, and become projectiles hurled at the container. Therefore this method is not recommended unless the weights can be permanently and reliably fixed in the rotor.

By supporting the rotor on a symmetrically mounted flexible (or "quill") shaft or magnetic bearing, the rotor can spin about a point near its inertial axis after going through the first critical resonance. This allows some amount

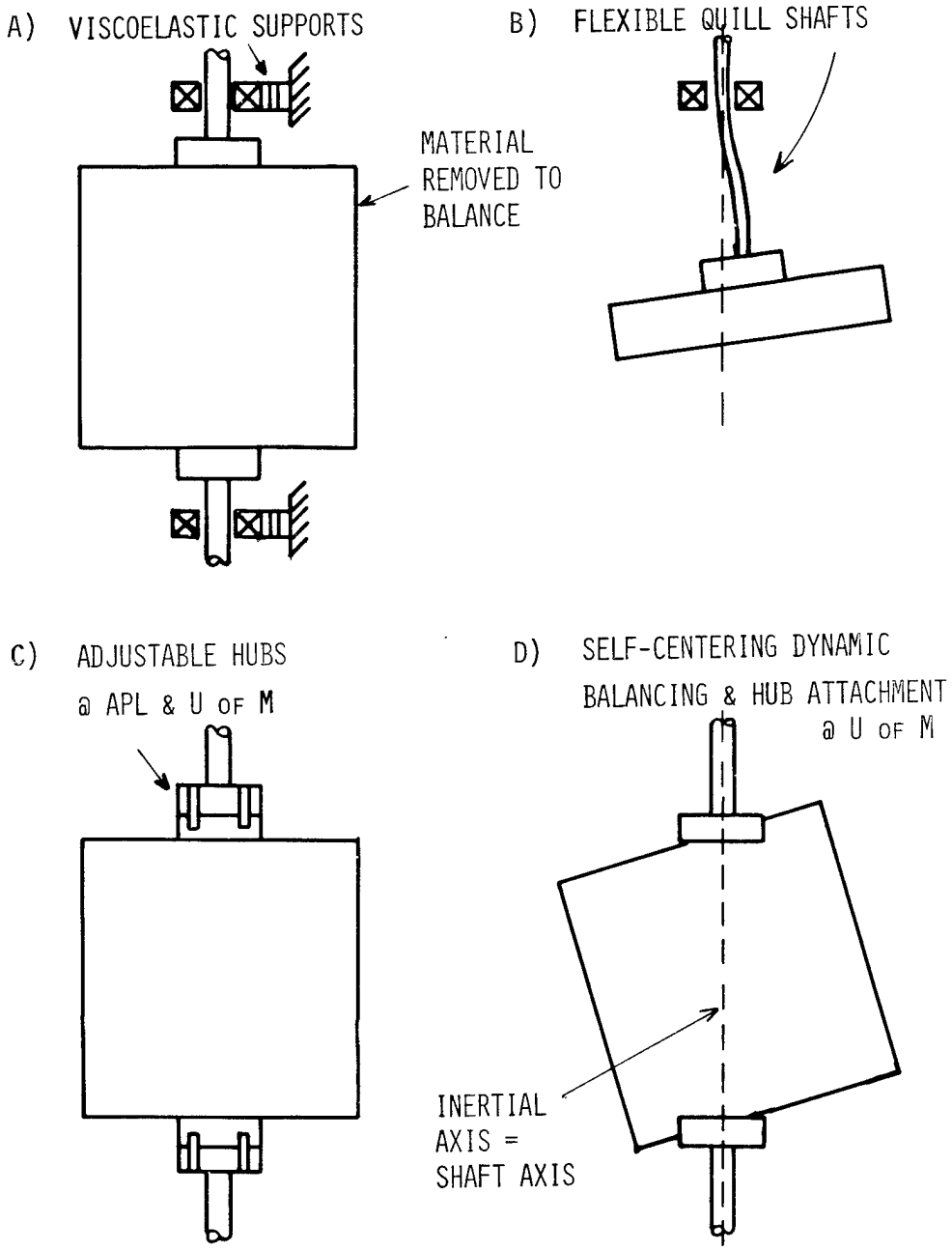

Figure 5. Rotor Imbalance Solutions

of imbalance to be tolerated in the rotor, and is the method currently used on most rotor tests.(4) (See Figure 5B.) Critical speeds that must be traversed and damping in the rotor can make the whirl problems particularly severe. The development of large multi-ton rotors implies much slower rotational speeds with higher torque requirements for the shaft, and thus less flexibility and higher stresses in the hub. Such large vertically mounted rotors may have to be supported by thrust bearings below the rotor. Permanent magnets may be useful to support the majority of the weight. (11) The bearings could be supported by very soft isolators to absorb a high degree of imbalance. The support system would have to be capable of sustaining the high amount of low level cyclic fatigue that would result (see Figure 5A).

Instead of removing or adding weight to the rotor to balance it, the rotor could be moved relative to the shafts so that the geometric axis coincides with the inertial axis of the rotor. The magnitude and location of the imbalance can be located by conventional methods of dynamic balancing. The results are interpreted in terms of displacement of the shafts instead of the amount of mass to add or remove. Adjustable hubs of this type have been designed and used in past programs at both the Applied Physics Lab and the University of Minnesota.(4,7)

A balancing apparatus to align the inertial axis of the rotor with its hubs and shafts was designed at the University of Minnesota under the present contract.(7) This apparatus provides the required four degrees of adjustment and has the advantage of greater sensitivity over incorporating adjustment screws in the hubs. It is also amenable to very large rotors.

2. Self-Centering Dynamic Balancing

Traditional balancing methods require measurement of the imbalance forces or displacements, and an active compensation by mass removal or

addition, or by shaft position adjustment. To eliminate the sensing, calculation and adjustment steps required in these balancing methods, a passive scheme was conceived to dynamically locate the inertial axis of the rotor and attach the hubs to the rotor with the shafts aligned and concentric with this axis. The design and development of such a balancer was proposed under the present contract, with the view that it might be simpler, less expensive, and directly suitable to pseudoisotropic rotors and especially to compound wound rotors. It would also eliminate the removal or addition of mass to a rotor and the associated potential stress concentrations.

The basic principle of this balancing method is to dynamically locate the principle inertial axis, and then attach the hubs with the centerlines of the shafts aligned parallel and concentric with that axis. The principle involved in locating the inertial axis in this self-balancing method, is that a rotor supported on isolators will tend to spin about its inertial rather than geometric axis if it is well above the fundamental resonance frequency. (See Figure 6) This inertial axis can then be marked, and the hubs attached to the rotor concentric to the inertial axis when stationary. A further possibility is to attach the hubs to the rotor while it is spinning about its inertial axis which then coincides with the geometric axis of the balancing equipment. Equipment to accomplish this was designed in this project, and is described as follows.

The basic design consists of an upper and lower turntable, eight visco-elastic-foam rotor support pads, a framework and a power source (Figure 7). The turntables provide a mounting surface for the rotor supports. The lower turntable is supported by two large spherical roller bearings. The bearings are pressed onto a vertical shaft from the turntable to provide the necessary radial alignment and axial support. Clearance is provided in the center of

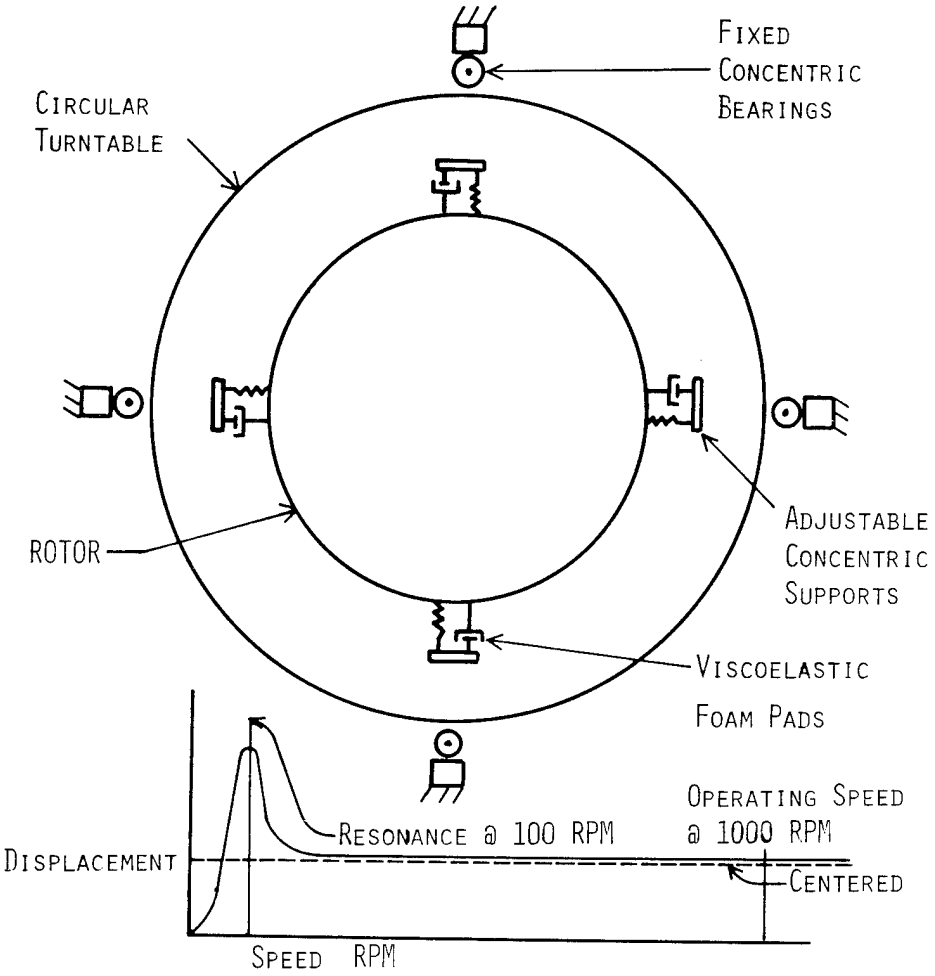

ROTOR CENTERS ITSELF WITH IT'S PRINCIPAL AXIS OF INERTIA ALIGNED PARALLEL AND CONCENTRIC WITH THE TURNTABLE'S GEOMETRIC AXIS.

Figure 6. Self-Centering Dynamic Balancer, University of Minnesota, 1979

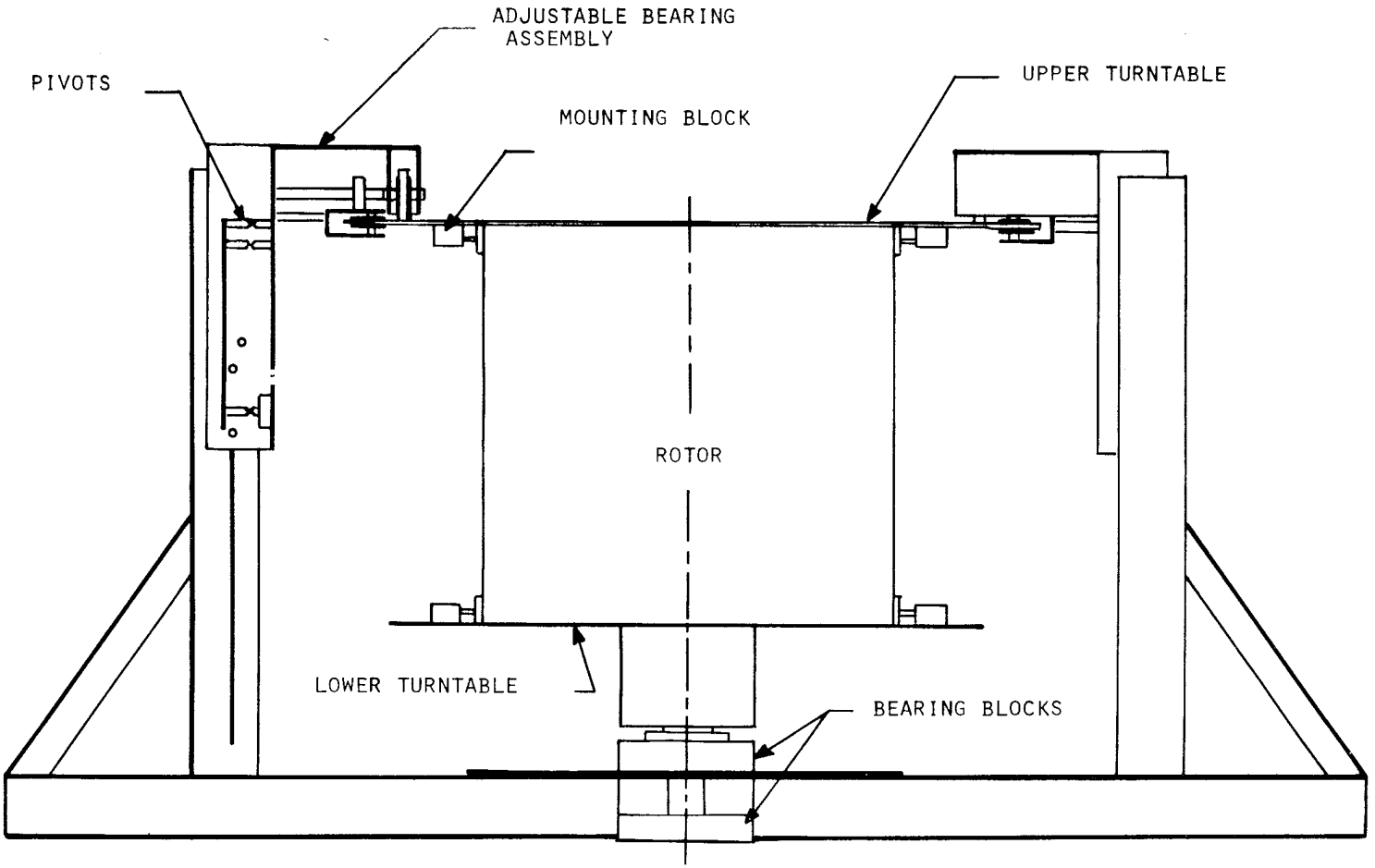

Figure 7. Self-Center Dynamic Balancer

che table for a hub-and-shaft mounted on the rotor. Four adjustable supports are mounted on each turntable. The supports provide the surfaces for mounting the viscoelastic foam pads.

The same basic turntable-support arrangement is used on the upper turntable with several modifications. Because the center of this turntable has to remain unobstructed to allow a friction pad to contact the rotor, a thrust bearing could not be used. Instead, eight side-mounted roller bearings are used to support and align the upper turntable both radially and vertically. The four side-bearings which provide radial alignment of the axis are adjustable to within .0025 inches. Two of the side-bearings could be instrumented using two force-transducers to measure the imbalance forces encountered as the rotor is spun up.

A surrounding framework is provided to mount the bearings supporting the turntables and a safety screen. The bottom turntable may be powered by an electric motor through a belt drive in order to bring it up to speed and to maintain the proper speed of the rotor while the surface is being sanded. A brake is attached to the shaft on the lower turntable to stop the system.

The viscoelastic-foam pads which are mounted on the turntables restrain the rotor while permitting it to align itself with its inertial axis, i.e., the foam acts like a parallel spring-and-damper combination. A number of different grades of highly viscoelastic foam are commercially available ranging from very soft to very stiff. (11) Samples of the different grades of this foam were tested for their stiffness in compression. The foam has a nominally linear region initially before the stiffness rises rapidly as it is completely compressed. (See Figure 8) This performance is temperature dependent. The resonance frequency of the rotor-balancer system is

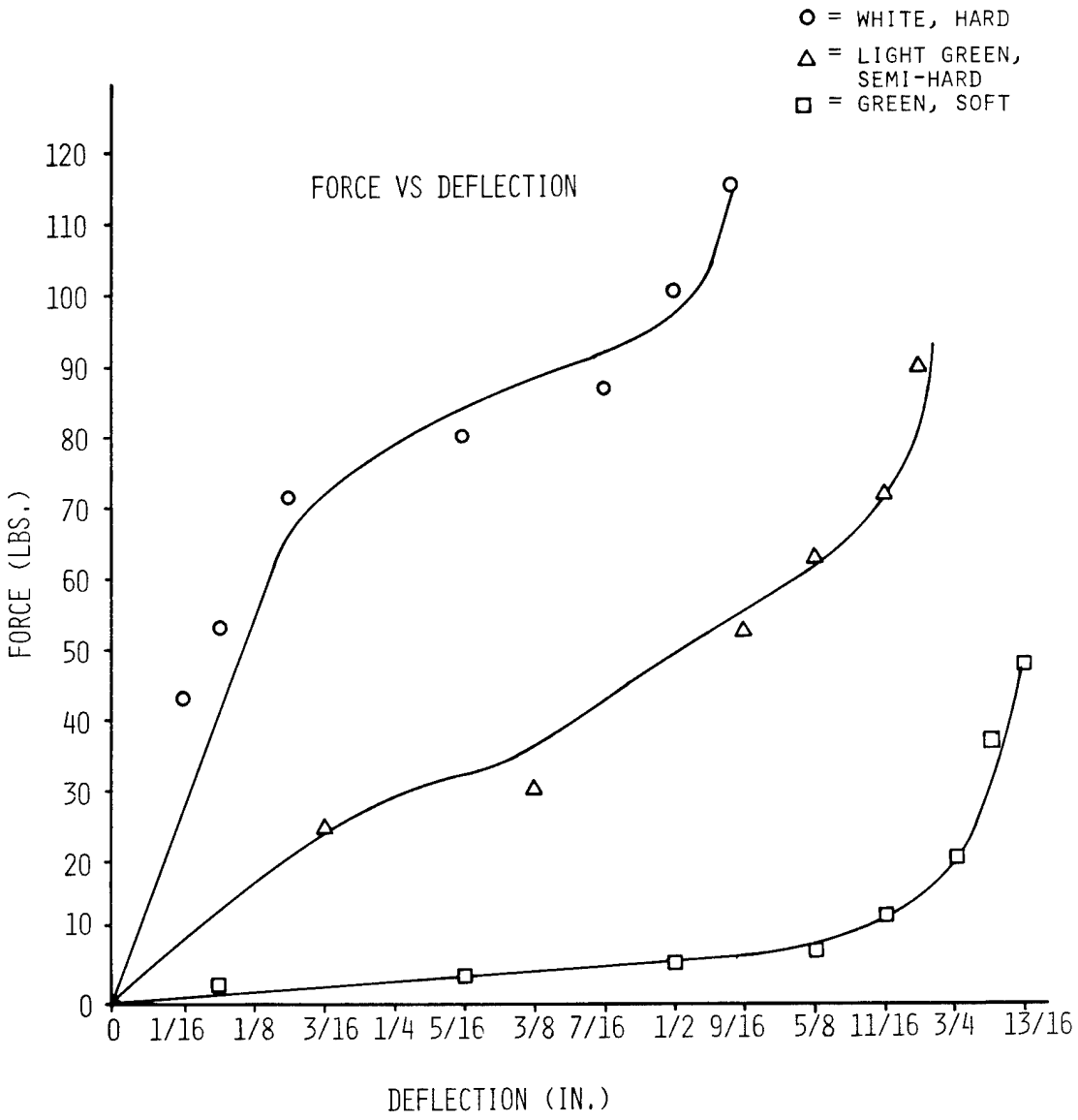

Figure 8. Force Vs. Deflection For Viscoelastic Foam

governed by the rotor mass, and the equivalent spring-constant of the foam pads, i.e., their area multiplied by their stiffness. The resonance frequency should be chosen well below the maximum operating frequency of the balancer to permit as close an alignment as possible between the rotor's inertial axis, and the turntables' geometric axis (see Figure 6). This viscous-damping of the foam controls the amplitude of the resonance, as well as the degree to which the inertial axis approaches the geometric axis. There is an optimum damping coefficient. Since most materials have damping coefficients considerably below this optimum value, the damping should be chosen as high as possible.

This entire self-centering dynamic balancer was designed to be installed on the bed of a large radial arm drill press with a 1.2 m (4 ft.) radial clearance, which is available in the Mechanical Engineering department. The apparatus is designed to accommodate rotors up to 710 mm (28 in.) in diameter and in height about a vertical axis. The apparatus will be bolted to the bed of the drill press, and then the eight bearing blocks adjusted so that the turntables' rotational axes would be aligned with the spindle axis of the drill press.

To balance a rotor, a friction pad is chucked into the spindle press and brought into contact to the top of the test rotor and is used to spin the rotor up through the fundamental resonance speed until it is spinning smoothly about its inertial axis well above that resonance speed. The design resonance and operating speeds are 100 RPM and 1,000 RPM respectively. The friction pad is then used to lightly sand a flat surface on the top of the rotor which will allow the hubs to be mounted concentric and perpendicular to the principle inertial axis. The friction pad would then be replaced by the actual hub and shaft. There is also the possibility that these could

be bonded directly to the rotor at the balancer operating speed while the rotor's inertial axis is aligned with the balancer's geometric axis.

The viscoelastic foam has been obtained in a number of stiffness grades and in thicknesses of 7 mm, 4 mm and 2 mm (1/2", 1/8" and 1/16"). The materials for the framework and the turntables have also been obtained. Construction of the apparatus was begun, but terminated due to lack of time and funds to complete it.

The essential development of this self-centering dynamic balancer is complete. Some modifications and optimization may be necessary when its construction is completed, and it is tested. The equipment should enable the rotor to be balanced as the hubs and shafts are attached, without having to add or remove mass later. This concept could be combined with the use of adjustable hubs. This balancer could conceivably be modified to manually align rotors with adjustable hubs.

The corollary to balancing a rotor using this self-centering method, is to provide the rotor with automatic-balancing hubs. Such hubs would contain some highly viscous fluid in a cylindrical ring. Since the rotor will be primarily operating above the transverse critical frequency, this fluid will move around to automatically compensate for any remaining imbalance in the rotor. Such a system would continuously balance the rotor, and compensate for any possible growing imbalance caused by uneven creep of the rotor material. Such balancing techniques are commercially available, and could be easily adapted for use on pseudoisotropic rotors and cores.

These balancing and assembly concepts should enable any flywheel rotor with a pseudoisotropic core to be balanced without having to add or remove mass. The automatic-balancing hubs would maintain the balance in the rotor by compensating for minor shifts in the rotor's center of gravity.

C. ROTOR VIBRATIONS

To maximize usefulness and minimize cost, flywheels need to be operated over the widest practical speed range. The critical frequencies encountered pose the greatest difficulty to such operation. The supports and operating range must be designed to avoid and minimize these resonances. The following parametric analysis discusses the basic design factors involved in choosing maximum operating speed and the fundamental translatory frequency. (13)

The purely translatory undamped natural critical frequency ω_c of a symmetric rotor of mass M is:

$$\omega_c = (K_e/M)^{\frac{1}{2}} \tag{1}$$

where K_e is the equivalent spring constant of the support system with elastic center at the center of gravity.

The energy stored in such a rotor with a moment of inertia I at its operating speed ω_o is:

$$E = I\omega_o^2/2 \tag{2}$$

Combining these equations, we find that the square of the ratio of the maximum operating speed to the critical speed is:

$$\left(\frac{\omega_o}{\omega_c}\right)^2 = \frac{2\ M\ E}{I\ K_e} \tag{3}$$

The maximum energy that can be safely stored in a rotor can be expressed in terms of the useable design strength of the rotor material σ_u and its density ρ as:

$$E = M\ K_m\ \sigma_u\ /\rho \tag{4}$$

where the mass shape factor K_m varies from zero to one depending on the stress distribution in the rotor. Substituting this expression for the

energy into equation (3) we have:

$$\left(\frac{\omega_o}{\omega_c}\right)^2 = \frac{2M^2 K_m \sigma_u}{I K_e \rho} \qquad (5)$$

Rearranging this equation and simplifying, we obtain another dimensionless parameter:

$$\frac{\sigma_u L}{K_e} = \frac{I L}{2 MVK_m} \left(\frac{\omega_o}{\omega_c}\right)^2 \qquad (6)$$

where V is the volume of the rotor. The ratio IL/MVK_m is a function of the mass distribution within the rotor, and is thus dependent on the rotor configuration. The ratio of operating to critical frequencies is defined by the choice of continuously variable transmissions and relative operating region. This dimensionless parameter can therefore be used to specify the equivalent spring constant desired for a specified rotor and operating conditions. It could therefore be called the "support parameter".

Let us consider a hollow cylindrical wound rotor of outer radius R_o, length L, with the ratio of inner to outer radius as X. The volume of this rotor is

$$V = \pi R_o^2 (1 - X^2) L \qquad (7)$$

Its moment of inertia I is

$$I = MR_o^2 (1 + X^2) / 2 \qquad (8)$$

and the mass shape factor K_m is

$$K_m = (1 + X^2) / 4 \qquad (9)$$

Substituting equations (7) to (9) into equation (6) we have

$$\frac{\sigma_u L}{K_e} = \frac{1}{\pi(1-X^2)} \left(\frac{\omega_o}{\omega_c}\right)^2 \qquad (10)$$

Typically an operating range of the order of 1:3 is desirable to make the maximum use of the energy stored in the rotor within the operating limits of the continuously variable transmission. The operating speed must be significantly above (or below) the fundamental transverse critical frequency. If we take the minimum operating speed as more than a third higher than the critical frequency, then the maximum operating frequency would have to be more than four times higher.

$$\omega_o / \omega_c \geq 4 \tag{11}$$

The ratio of inner to outer radius X is chosen to optimize the energy storage costs of the rotor. (6) Taking a typical inner to outer ratio of 0.8 the support parameter becomes

$$\frac{\sigma_u}{K_e} L \geq 14.2 \tag{12}$$

The required stiffness in the rotor supports can thus be chosen based on the size of the rotor and the useable material strength. Low operating speeds are desired to minimize bearing surface speeds. This suggests a large rotor diameter and short length which would require softer supports.

For a solid pseudo-isotropic rotor the inner radius, and thus X, is zero for equations (7) and (8). The mass shape factor could be taken to be 0.25 until further data is available relative to the unixial strength. The support parameter for cylindrical pseudoisotropic rotors is thus

$$\frac{\sigma_u}{K_e} L \geq 20.4 \tag{13}$$

This support parameter appears to be a useful parameter in the initial design of a flywheel energy storage system. It allows the equivalent spring constant of the supports to be quickly chosen based on the useable strength of the rotor material, and the rotor length, for a given rotor configuration.

To measure the fundamental critical frequency of a rotor and supports, an experimental plywood was mounted in brackets on an electromagnetic shaker. The transmissibility curve was measured and is shown in Figure 9. The nominal operating range of such a system is indicated on the figure.

A first order linear analysis of the individual spring constants and the major vibratory modes was made for the above system by Carlson. (14) The critical frequencies calculated are of comparable magnitude to these experimental results. The major uncertainties were in the moduli and damping coefficients of the elastomeric pad and of the bearing isolators. Measurements of these parameters could be made in further testing to refine the coefficients.

In operating above the fundamental critical frequencies, serious consideration must be given to whirl frequencies and to the magnitudes of such vibrations. Detailed analysis of the whirl frequencies and vibrations of flywheels have recently been made by Bert and Chen. (15) Further analysis of these effects has been made by Bucciarelli, concentrating on the effects of damping in the rotor as well as in the bearing isolators. (16) Damping in the rotor tends to amplify the whirl modes, indicating that a rigid rather than elastomeric mount between the hub and rotor may be desired. Preliminary arrangements have been made to apply this analysis to the plywood rotor that has been designed and built at the University of Minnesota.

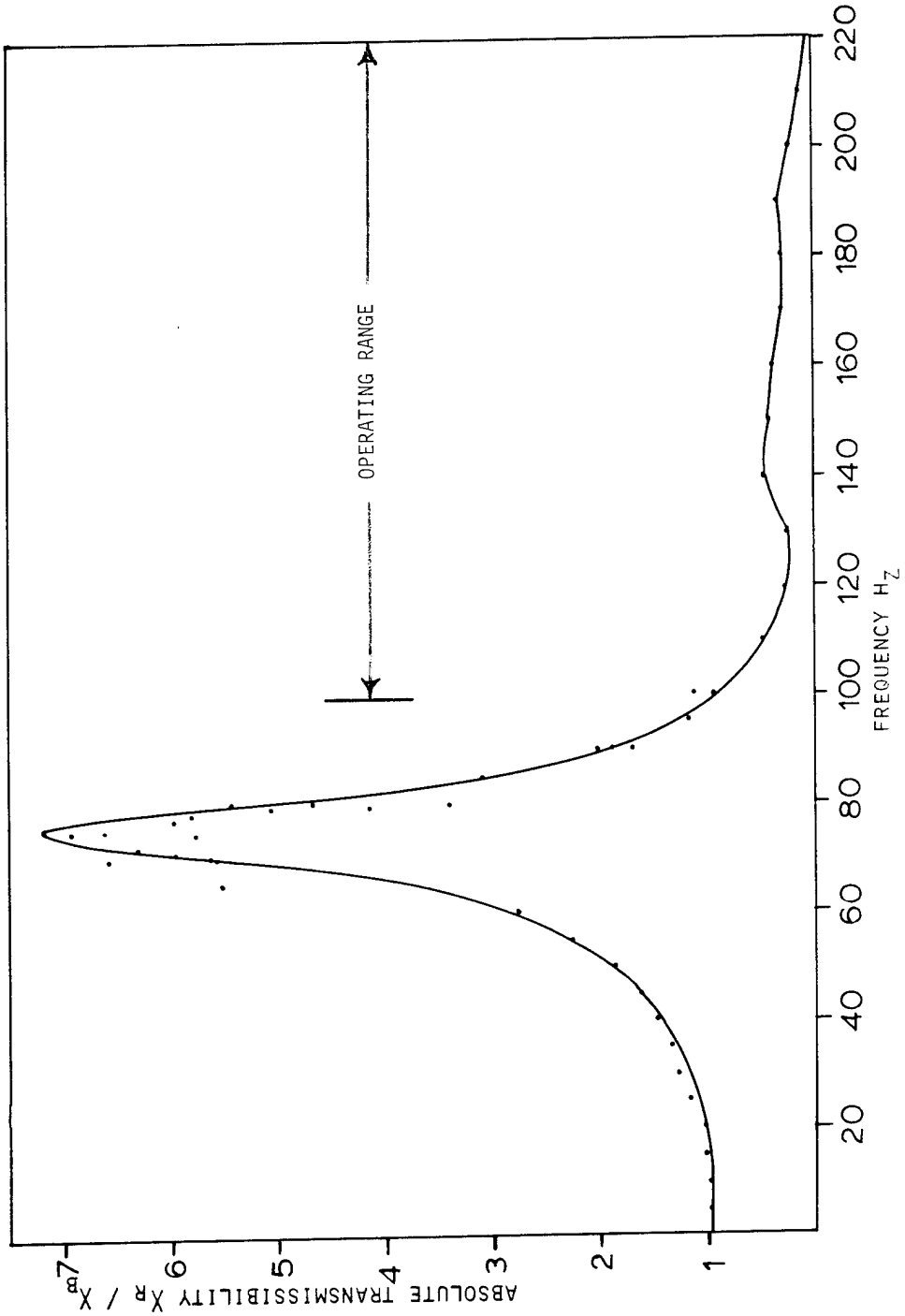

Figure 9. Transverse Transmissibility of Plywood Rotor

The magnitude of these effects could be measured and changed experimentally to compare them with the analytic results.

This preliminary transmissibility data was taken manually. However the output from the accelerometers has since been connected directly to the amplifiers and then to the microprocessor based data acquisition system that has been assembled. This enables measurements of the phase as well as magnitude of various points in the system. Log decrement experiments can thus be made easily and accurately. At present the quantity of data that can be taken rapidly and stored is limited by the 8K words of memory.

II. MATERIAL PROPERTIES AND ROTOR DURABILITY

The basic design of a flywheel energy storage system requires that it meet specified power and energy storage capabilities for a given period of time. The design of the power and torque transmitting capabilities of the rotor are shown in Figure 10. The hub must be able to transmit the maximum power at the minimum design speed, which is typically set above the fundamental critical speed. This in turn is designed to be some fraction of the maximum useable operating speed. The hub must also be able to sustain the stresses resulting in transversing the critical speeds as well as the stresses experienced under continuous operation.

The design of energy storage capabilities of the system are similarly shown in Figure 11. The specific energy (per unit mass) storage capabilities of the rotor material are given by $\hat{E} = K_m \sigma / \rho$ where K_m is a shape factor varying between 0 and 1 accounting for unequal stress distributions, σ is the tensile strength of the material, and ρ is its density. The mean strength of the material over the operating cycle and life of the system is reduced through fatigue by a factor f. There is also a distribution of strengths in the material. To design for a given confidence level (e.g. 95% confidence limits), the distribution of strengths of the material must be known (e.g. 2 standard deviations below the mean for a normal distribution). Finally the operating range of the continuously variable transmissions in the drive train or the torque limitations at the design power level constrain the lower limit to which energy can be withdrawn or added to the rotor. This is accounted for by a speed ratio factor W equal to the percentage of energy that can be extracted from the rotor.

To evaluate the feasibility of using cellulosic materials to make

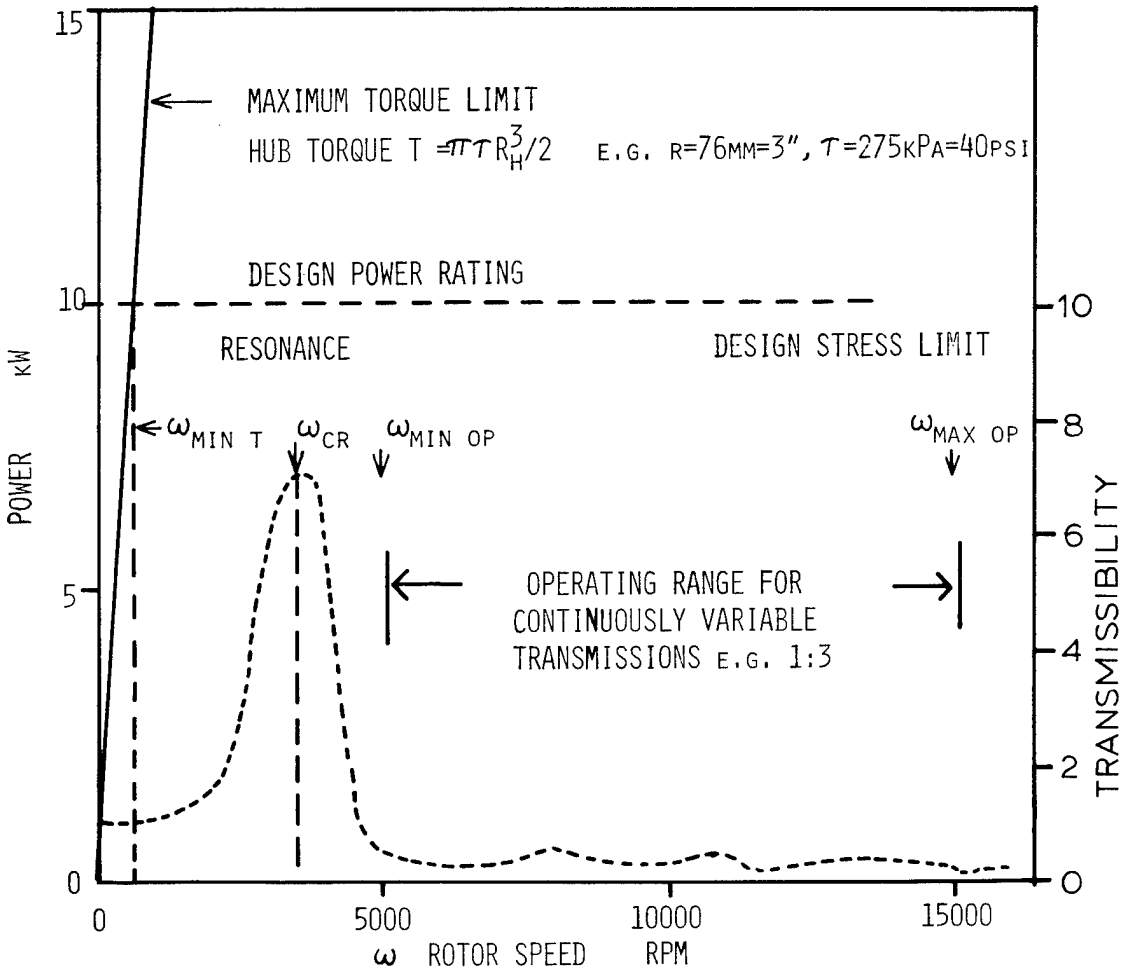

Figure 10. Power and Speed Design

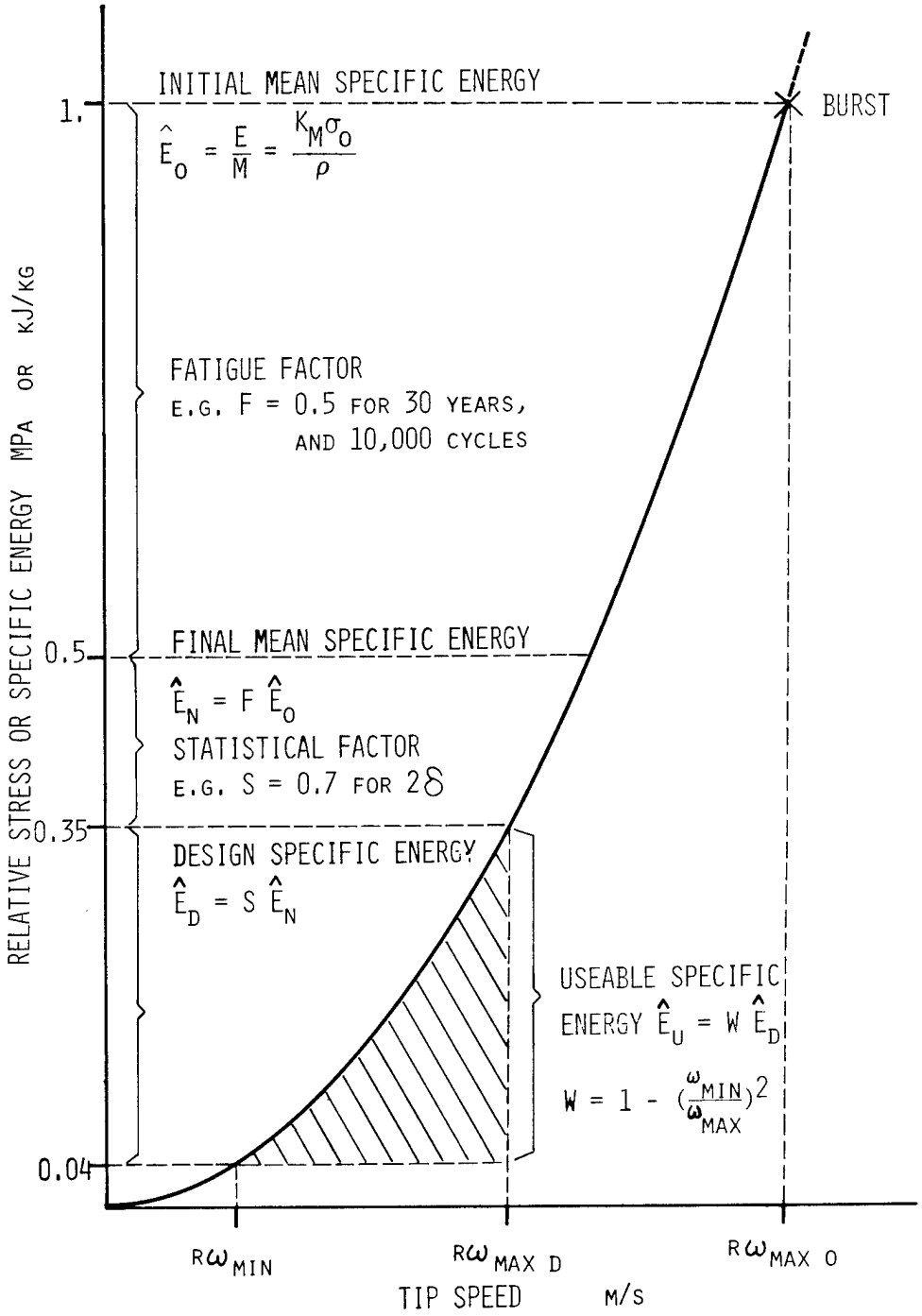

Figure 11. Useable Energy Design

flywheel rotors, it is therefore necessary to evaluate the distribution of strengths of the material in question, and the effect of fatigue on it. This project therefore sets out to evaluate in sufficient detail these factors for birch plywood, as this material is commercially available and could conceivably be used in rotors, based on literature studies and on actual tests of plywood rotors. Four types of tests were therefore proposed.

(A) Tensile tests to establish the strength distribution of plywood.

(B) High resolution rapid tensile tests with acoustic emission measurements to attempt to predict the long term strength.

(C) Tensile fatigue tests of plywood.

(D) Durability of the rotor-hub system, under cyclic rotary fatigue.

These tests would be run for plywood under ambient conditions for 50% Relative Humidity as well as for vacuum dried material, to enable evaluation of data currently in the literature.

A. TENSILE TESTS

To evaluate the specific energy of the plywood, the tensile strength-to-density ratio distribution must be known as well as the shape factor K_m. It would be preferable to have information on the statistical distribution of the intrinsic energy density after the material has been subjected to the stresses expected under normal rotor operating conditions. Such data is very difficult to obtain and time consuming. Much information can, however, be obtained rapidly through standard tensile tests of numerous samples. This information can then be compared with fatigue tests to progressively longer periods and lower stresses in order to extrapolate the data to the expected life cycle stress conditions. Such tests can also be used to identify problems of material selection and quality control in the manufacture of cellulosic rotors. This is particularly important since most plywood is not made to meet stringent standards required for such high performance engineering standards.

Wood is very hygroscopic in nature and also shrinks and swells with changes in moisture content. The strength increases as the wood is dried from the green moisture-saturated state down to ambient conditions. At 50% relative humidity (RH), the moisture content is typically 10% depending on species. Most data in the literature on the strength of various species are measured at ambient conditions, with some data taken at the fiber-saturated point. Little data exists for very dry wood or plywood, and the reports are sometimes conflicting. There is some indication that data indicating lower strengths was left out (17). Measurements of individual tracheids of Douglas Fir show reductions in the strength when they are dried down from ambient conditions.

Plywood is considerably weaker in tension along the direction bisecting the grain directions of adjacent plies than in the direction of those plies.

For example, the strength at a 45° angle to the face ply of conventional 0°, 90° plywood is significantly weaker than parallel or perpendicular to the face grain. This region may be the weakest in the rotor, precipitating failure of the entire rotor when it fractures. Little data are available along these directions compared to parallel and perpendicular to the face grain. The shape factor K_m is used to account for nonuniform stress distributions in the rotor. A solid cylindrical rotor of isotropic material has a shape factor of 0.606 for example. K_m could be used to reflect the effects of grain orientation and/or lamination pattern in mathematical equations used to calculate the usable strengths of various wood-species in both solid and plywood form.

Primary Goals

The testing program was therefore designed to evaluate these three major factors of intrinsic energy distribution, moisture effects, and plywood orientation. To evaluate the intrinsic energy distribution accurately it was decided to test at least 50 samples and preferably 100 samples in each series. The different orientations would be tested with material that was vacuum dried and also with material conditioned to 50% RH to evaluate the moisture effects. Finally, tests would be run on plywood parallel to the grain and at the angle bisecting the grain angle in adjacent plies. Commercially available Finnish birch plywood was obtained and 450 tensile samples were cut for these series of tests.

Calculations and burst tests indicate that pseudoisotropic material made up with a 0°, 60°, -60° configuration is considerably stronger than if made in the conventional 0°, 90° configuration (8). Preliminary tests and discussions with the plywood distributors indicated that there might also be further effects of quality control and hot press versus cold adhesives in

reducing the strength of commercially available birch plywood. An order for 75 sheets of birch plywood 460 mm (18") square made with a 0°, 60°, -60° veneer orientation was therefore placed with Lenderink Inc. of Belmont, Michigan (18). As a control, 25 similar sheets were ordered with a conventional 0°, 90° orientation.

Some of the sheets will be used for fatigue tests. Six sheets of the 0°, 60°, -60° plywood were sent to the Applied Physics Laboratory for future burst testing to compare actual spin tests with this series of tensile and fatigue tests.

Experimental

Initial tensile tests were made on 12 mm (1/2") Russian "Baltic" Birch plywood which was available from a local lumber distributor (19). Tensile samples were routed out using a jig that was already available. Many of these samples failed outside the gage length. The jig outline apparently had too sharp a curvature and made the gage section too wide to adequately distribute the stress. A new jig was therefore made to cut samples in a shape that aproximated the ASTM plywood tensile specimen standard. The actual dimensions had to be 25% shorter to accommodate the limitations of the environmental chambers available. These are still considered to provide relative measurements of the various effects. (See Figure 12)

The Baltic birch is assembled using urea adhesives. Numerous blemishes are generally present in the interior of this plywood, even when the face veneers are relatively clear. Subsequent tensile tests were therefore made on a higher quality birch plywood from Finland, which was obtained through a distributor in Chicago (20). This plywood is made using phenolic adhesives in a hot press, and is of exterior or water resistant quality. It has specified minimum strengths for use as concrete forms. The plywood is

Figure 12. Plywood Tensile Test Samples

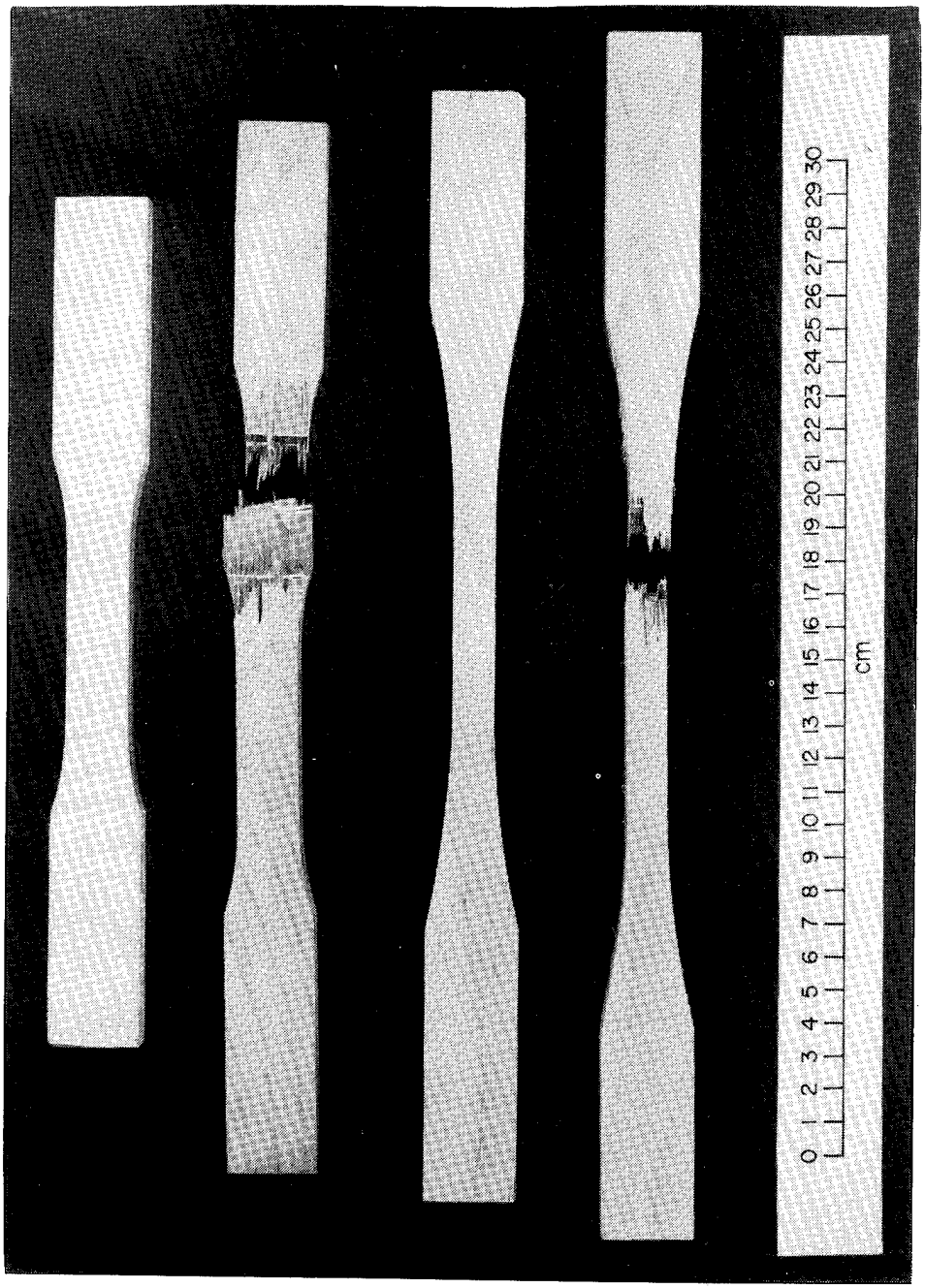

Early samples made with an existing die.

Final tensile samples made with the new die.

The original die had too sharp a routed radii and too thick a gage section. The new die was made with a larger 11" radii and ½" thick gage section. This has given samples breaking consistently in the gage section.

nominally 12 mm (0.5") made up of 9 plies.

The custom-made boards from Lenderink Inc. were assembled with 16 veneers of 0.9 mm (1/28") thick of yellow birch. The boards with the 0°, 60°, -60° were made using cold setting aliphatic polymer resins. These were used to avoid possible material degradation and delamination problems with the hot setting adhesives. The control plywood was made of 15 plies of the same material with a conventional 0°, 90° orientation. Part of it was made with cold setting adhesives and part with hot press adhesives to compare this parameter.

Sample Preparation

For the tests of the conventional 0°, 90° Finnish birch plywood, 450 samples were cut from the 1,500 mm (5 ft) square sheets. Samples were cut with the grain of the face veneer at 0°, 45°, or 90° to the axis or tensile stress direction. The custom-made 0°, 60°, -60° plywood was similarly cut into tensile samples parallel and perpendicular to the face grain. The latter is at 90°, 30°, -30° to the other veneers and bisects the grain directions of the adjacent plies. Forty-three boards have been cut into 731 sample blanks for tensile and fatigue testing. Due to the dimensions of the boards, three samples were obtained parallel to the grain and fourteen perpendicular to the grain in each board or vice versa. For the fatigue tests, ten perpendicular samples were set aside from each board, along with the four perpendicular and three parallel samples used for tensile tests and as controls. (See Figure 13.) The sample blanks were then routed to shape.

For the tensile tests and moisture comparison tests, the samples were evenly distributed between two groups for separate conditioning. The first group was equilibrated to constant weight in an environmental room maintained

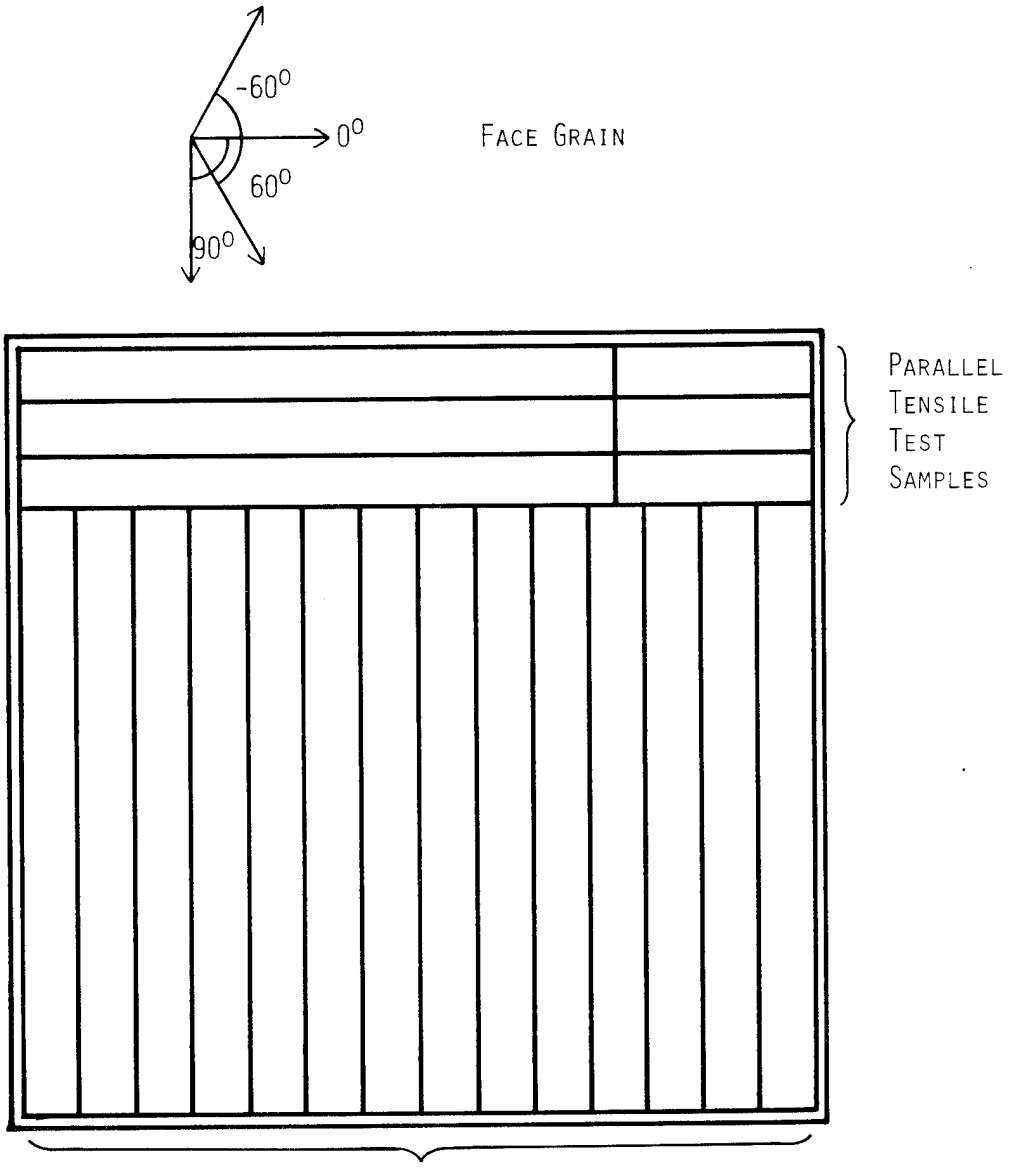

Figure 13. Test Blanks Cut From Hexagonal Plywood Squares

at a constant 22°C (72°F) and 50% RH. The second group was vacuum dried to constant weight in a vacuum environmental chamber. Upon equilibrium, the pressure in the chamber ranged from 1 to 8 Torr (microns of Hg), giving a moisture content close to 0% and comparable to that expected under flywheel rotor operating conditions.

Testing Procedure

After fabrication and moisture conditioning, the samples were tested in tension at a constant strain rate using an Instron test machine. Each sample was given an identification number indicating the type of test, number of plies, moisture content, face ply orientation, and sample number within that group. The width and thickness of the gage length were then measured and recorded. The samples were clamped in the tensile grips with 50 ft. lb. torque applied to the bolts. An extensometer was attached to the sample across a 51 mm (2") gage length.

The sample was then broken in tension by pulling the grips apart at a constant rate. The load-extension curve for the gage section was recorded automatically on the chart recorder during the test. The breaking load was obtained from the chart and the breaking strength calculated from the cross sectional area of the gage length.

The samples equilibrated at 50% RH can be easily tested in the Instron since the whole room is controlled to those conditions. However, wood is very hygroscopic and would rapidly absorb moisture after being vacuum dried if placed in these conditions. The dry tensile samples were vacuum dried in a vacuum environmental chamber which was then backfilled with dry nitrogen. The samples were then sealed in plastic bags under dry nitrogen while still in the chamber. These bags provide a temporary water free environment in which the dry samples can be transported to the testing facility four miles

away.

The bagged samples along with all necessary accessories were placed in an environmental box mounted in the Instron test machine such as to enclose the immediate test area. The box was made of plywood with styrofoam insulaiton. A plexiglass front plate contained two rubber gloved access ports to permit manipulation within the box. The box was sealed, with a valve and port for admitting dry nitrogen on one side and an exhaust port and pressure release on the other. The box was flushed with dry nitrogen to less than 10% RH and maintained as such during the test. The dry samples were measured to gain 0.4% moisture content per hour outside in 50% RH air. However, they were in the environmental chamber at less than 10% RH for less than 20 minutes before testing, and as such would absorb less than 0.1% moisture. Longer tests would have to be maintained under lower relative humidity.

Density and Moisture Content

Both density and strength are needed to evaluate the intrinsic energy density of the material. It is also necessary to evaluate the actual moisture content of the specimens tested, especially the vacuum dried samples, to ensure proper conditioning and testing. Immediately after testing, a coupon 28 mm (1-1/8") square was cut from each sample and weighed. Samples were exposed to the moist air for less than five minutes before weighing. The coupons were then placed in an oven and dried at 105°C to constant weight (2-4 days). Coupons were then reweighed and the initial moisture content calculated. The coupon volume was determined by first coating the samples with a thin coat of wax. The differential weight caused by immersing the coupon in a beaker of water is determined and the volume of the coupon cal-

culated assuming a density of 1 Mg/m^3 for the water, displaced. The dry density of the sample is thus calculated.

Results

The results of the tensile tests of the Finnish Baltic birch are shown in Figures 14, 15 and 16 for tests 0°, 90° and 45° to the face veneers respectively. The samples were sorted numerically according to their tested strength and the strength plotted versus rank. The means and standard deviations for both the vacuum dried samples and those equilibrated to 50% RH are summarized in Table 1. The results indicate that this commercially available material has very large distributions of strengths with standard deviations ranging from 12 to 22%. As initially anticipated, there was a significant drop in the tensile strength after vacuum drying the plywood, ranging from 5 to 20%. This drop ranges from 25 to 102% of the standard deviation of the strengths respectively. The few samples with very low tensile strengths could probably be readily detected through nondestructive testing methods or eliminated through proof testing.

Note also that the strength of the plywood at 45° to the plies is 29.0% and 30.5% of the mean tensile strength of the parallel and perpendicular directions for material equilibrated at 50% RH and that vacuum dried respectively. This compares with 16.6% predicted theoretically by superimposing the strengths of veneers calculated from Hankinson's formula (16).

$$\sigma_\theta = \frac{\sigma_{||} \cdot \sigma_\perp}{\sigma_{||} \cdot \sin^n\theta + \sigma_\perp \cdot \cos^n\theta} \qquad 1.5 \leq n \leq 2$$

where $\sigma_{||}$ and $\sigma_\perp$ are the veneer strengths parallel and perpendicular to the grain, and θ is the angle with respect to the grain. The value of n was chosen as 2. This indicates that there is some benefit from laminating, but

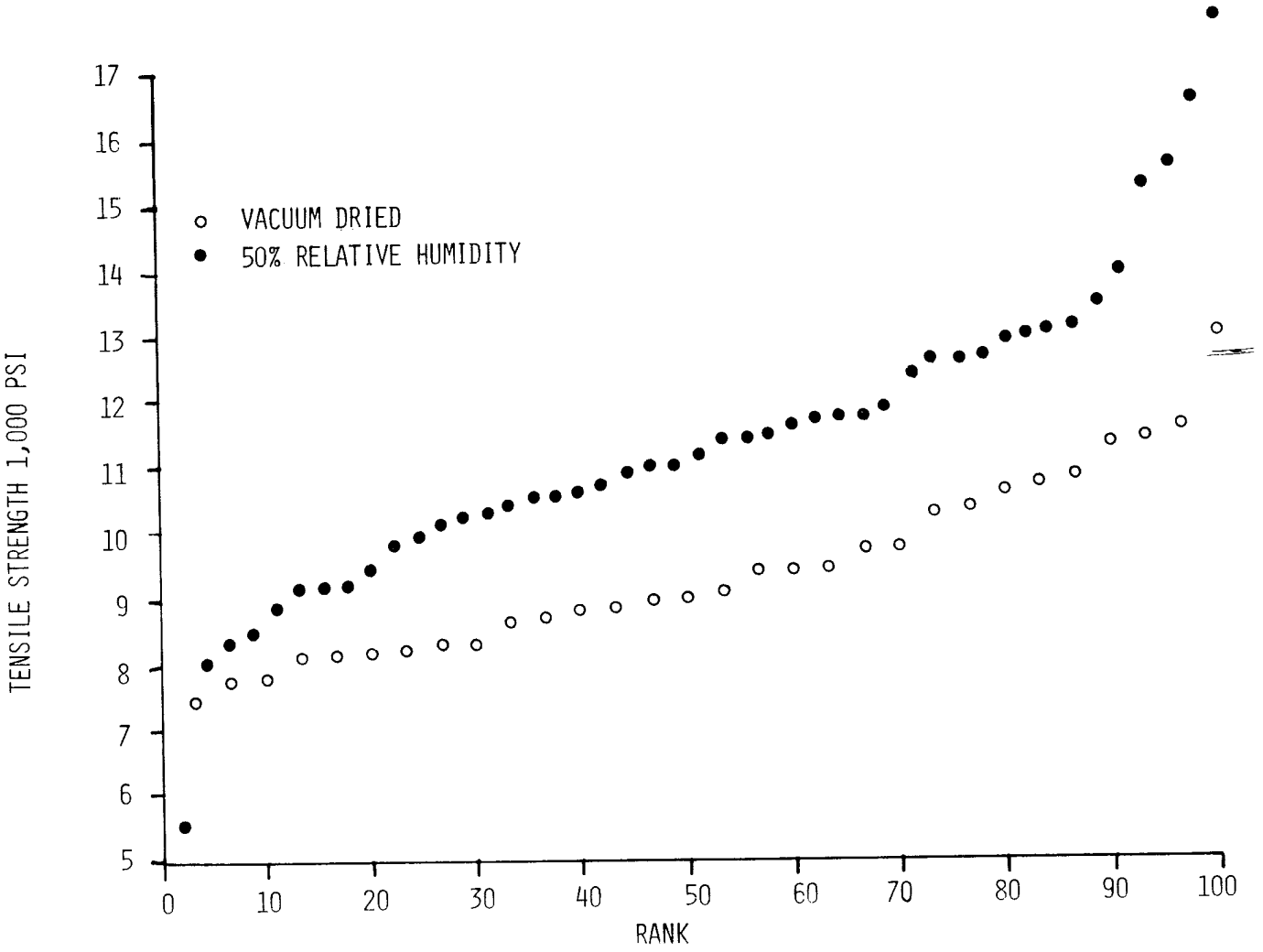

Figure 14. Tensile Strength of 0°, 90° Finnish Birch Plywood Parallel to Face Veneers

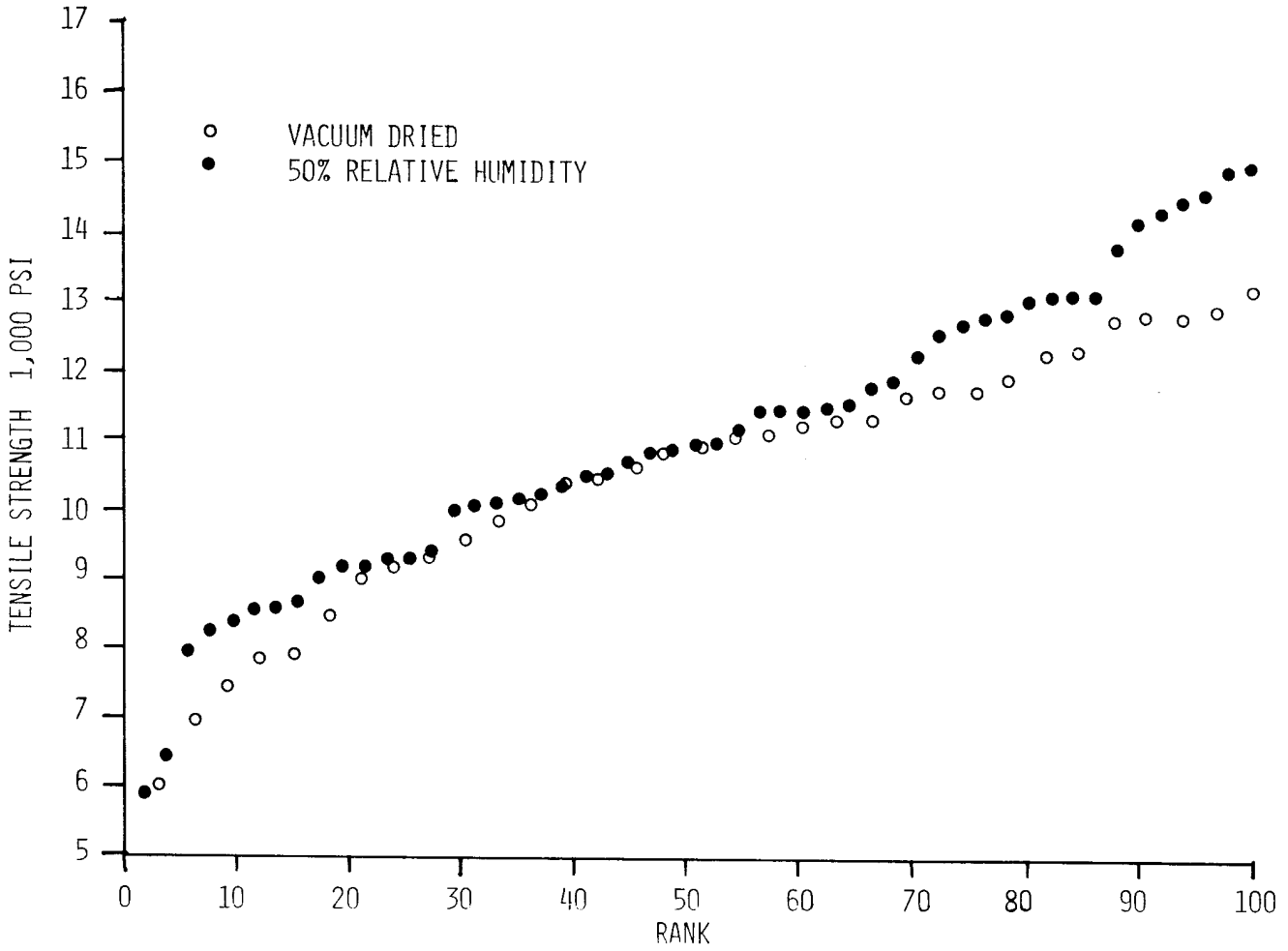

Figure 15. Tensile Strength of 0°, 90° Finnish Birch Plywood Perpendicular to Face Veneer Grain

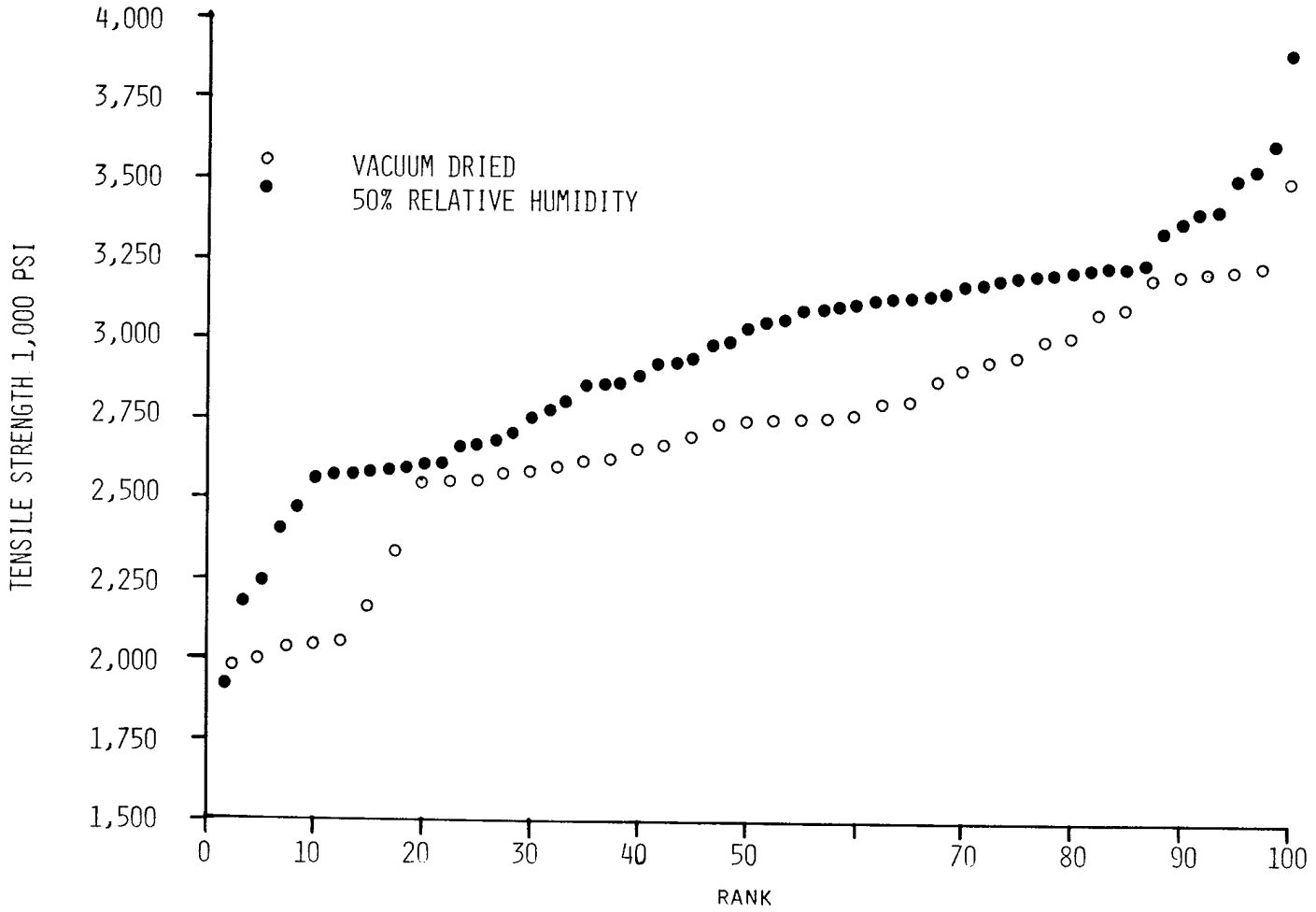

Figure 16. Tensile Strength of 0°, 90° Finnish Birch Plywood at 45° to Veneer Grain

TABLE 1. TENSILE STRENGTH OF 9 PLY 1/2" FINNISH BIRCH PLYWOOD

Face Veneer Orientation	RH%*	Number of Samples	Mean Strength MPa	Mean Strength Psi	Standard Deviation Psi	Standard Deviation D %	Drying Drop Δ%	Δ%/D%
Parallel	50	45	71.8	10,409	2,313	22.2		
= 0°	0	31	57.6	8,352	1,380	16.5	-19.8	-1.02
Normal	50	51	69.4	10,066	2,142	21.3		
= 90°	0	33	65.9	9,560	1,868	19.5	- 8.0	-0.6
Mid Ply	50	60	20.4	2,965	367	12.4		
= 45°	0	40	18.8	2,729	378	13.9	- 5.0	-0.25

* Samples equilibrated at 73°F and 50% relative humidity or vacuum dried to less than 20 millitorr pressure and tested in dry nitrogen atmosphere.

1 Psi = 6894.7 Pa

The ratio of the strengths at 45° to the average parallel and normal is 29.0% at 50% RH and 30.5% at 0% RH.

a more complete analysis is needed for accurate estimates (17).

Using similar calculations, plywood made with a 0°, 60°, -60° should have a theoretical strength along the directions 90°, 30°, -30° of 25.6% of that along one of the veneer directions. This is a 54% improvement over the situation with 0°, 90° plywood. Tests of the custom made birch plywood of this configuration are shown in Figures 17-20. The results are summarized in Table 2. Note that the mean strength and intrinsic specific energy values perpendicular to the face grain (90°) are 54.8% and 52.7%, respectively, of their corresponding values parallel to the face grain (0°). These percentage relationships represent an approximate 88% improvement in performance going from the cross ply configuration to the hexagonal configuration for the weakest direction in the plywood. The properties in this weakest direction are expected to correlate best with actual spin burst tests of disks of such pseudoisotropic material. Some reported spin tests of E-glass pseudoisotropic disks resulted in pseudo-isotropic strengths 34.6% and 45.6% of the uniaxial strengths, respectively, for cross ply and hexagonal ply construction (7). This was a 32% improvement for the tests performed.

The initial tests of the hexagonal plywood show a drop in strength when the material is vacuum dried similar to the conventional cross ply plywood. (See Figure 17). Part of this may be due to prestressing the material due to differential shrinkage. This effect is shown in the samples of the hexagonal plywood warping when they are vacuum dried. This situation exists because the hexagonal plywood has a helical geometry as compared to the cross ply material which is symmetrically constructed and does not exhibit such warping. The magnitude of this twisting effect is expected to be proportional to the change in moisture content from when it was manufactured to after it

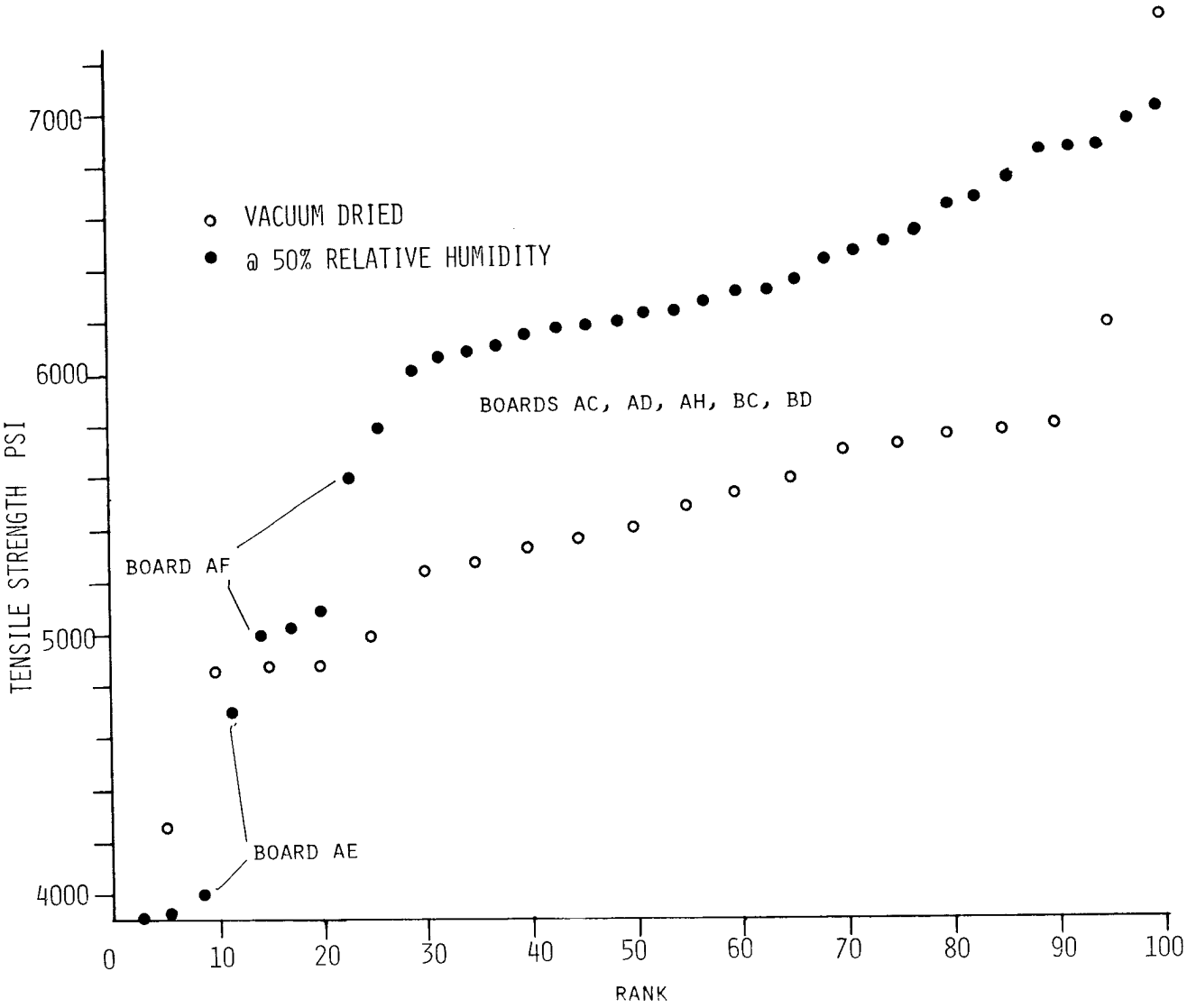

Figure 17. Tensile Strength of Hexagonal 16 Ply Yellow Birch Plywood Perpendicular to the Face Veneer Grain

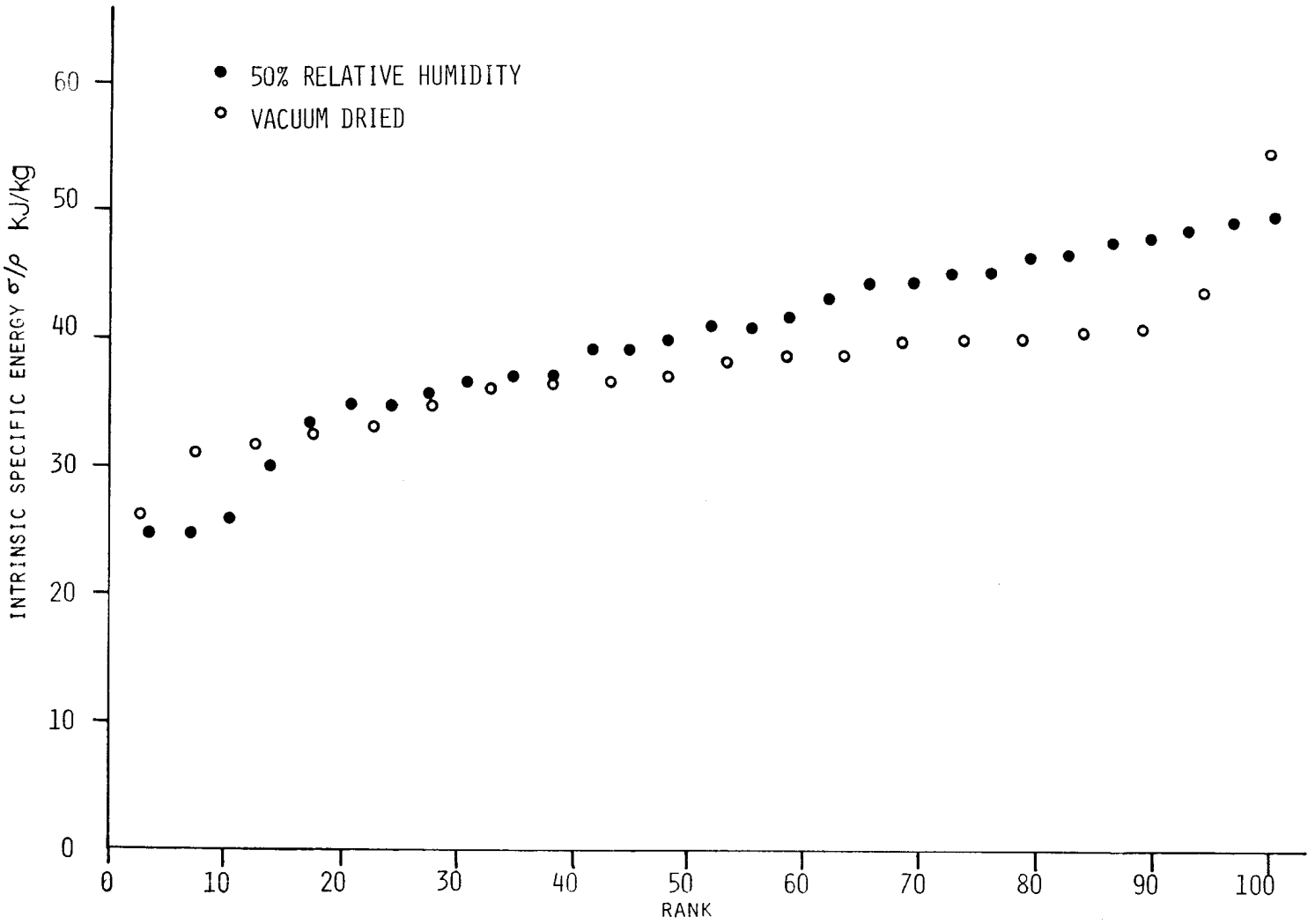

Figure 18. Intrinsic Specific Energy Distribution of Hexagonal Yellow Birch Plywood Normal to the Face Veneer

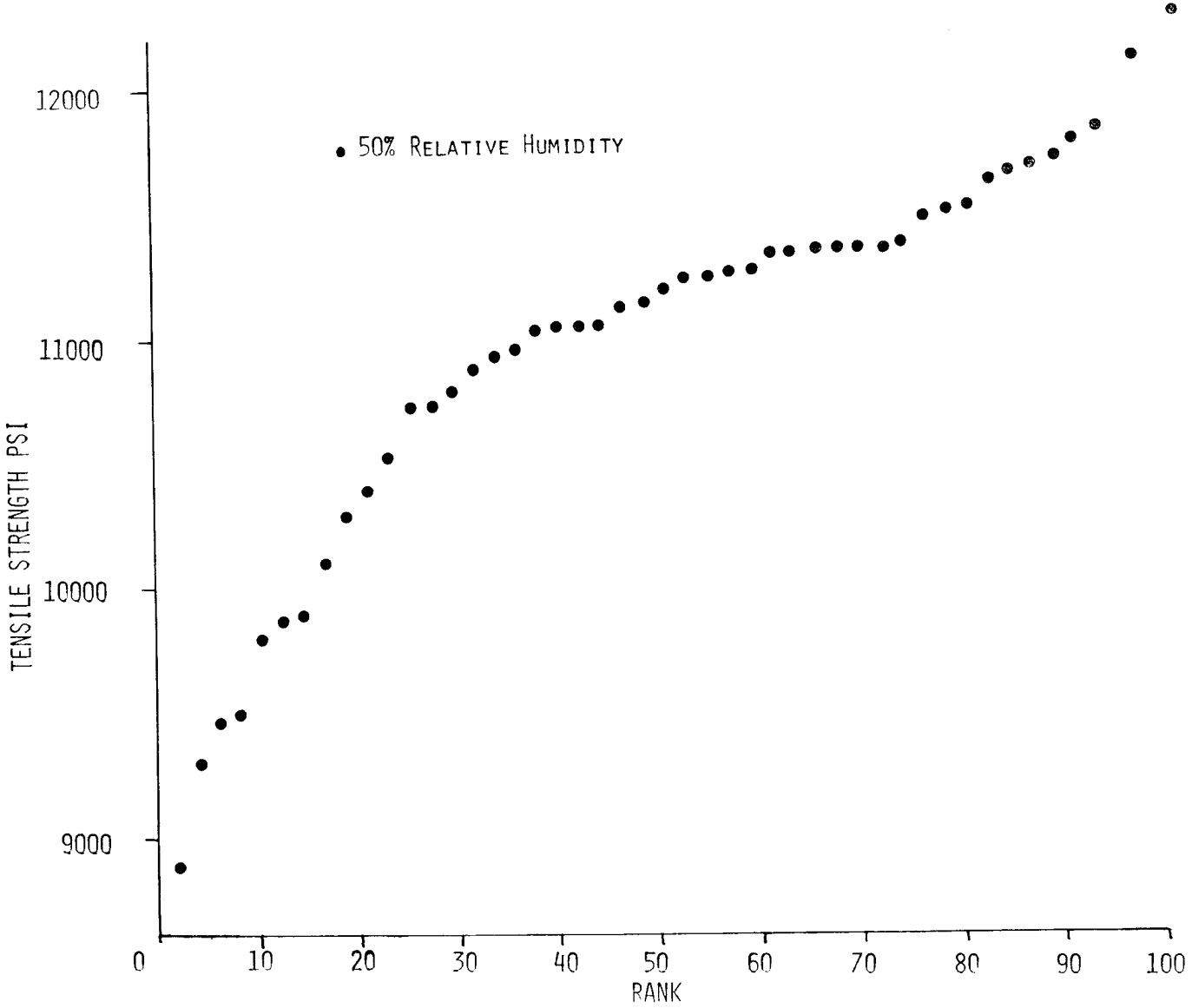

Figure 19. Tensile Strength of Hexagonal Yellow Birch Plywood Parallel to the Face Veneer Grain

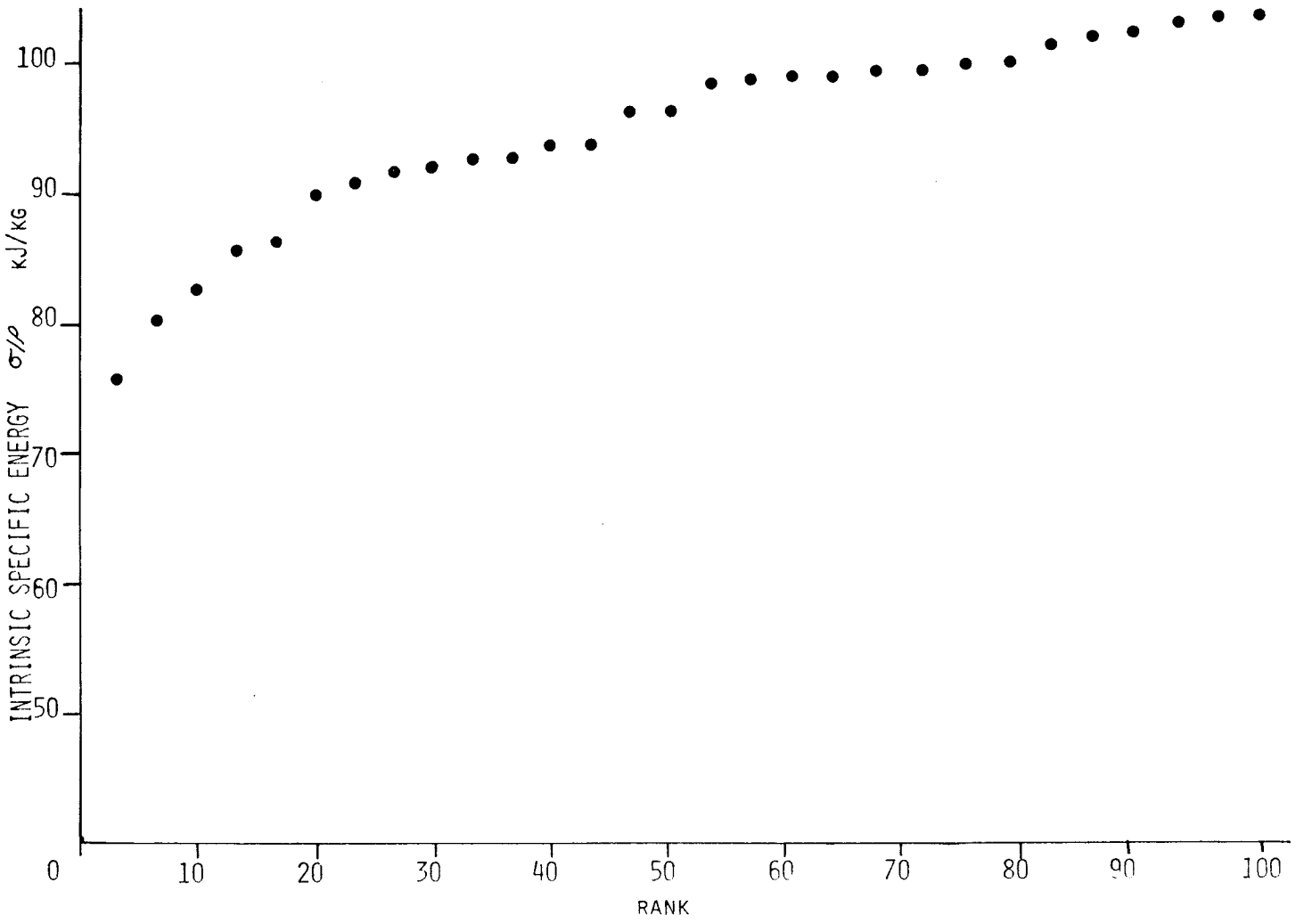

Figure 20. Intrinsic Specific Energy Distribution of Hexagonal Yellow Birch Plywood Parallel to the Face Veneer Grain

TABLE 2. TENSILE STRENGTH OF 16 PLY 1/2" HEXAGONAL YELLOW BIRCH PLYWOOD AND ITS INTRINSIC SPECIFIC ENERGY

Face Veneer Orientation	RH%	Number of Samples	Mean Strength MPa	Psi	Standard Deviation Psi	D%	Drying Drop Δ%	Δ%/D%
Parallel = 0^o	50	45	75.7	10,976	758	6.9		
	0	1	58.5	8,493	-	-	-22.0	-
Mid Ply = 90^o	50	35	41.5	6,019	853	14.1		
	0	20	37.8	5,488	640	11.6	- 8.8	-0.76

Face Veneer Orientation	RH%	Number of Samples	Intrinsic Specific Energy σ/ρ kJ/kg	Wh/lb	Standard Deviation kJ/kg	%
Parallel = 0^o	50	29	95.1	12.0	7.37	7.8
Perpendicular = 90^o	50	26	50.1	6.31	7.34	14.6

The ratio of the mean strengths perpendicular to parallel at 50% RH is 54.8%. The ratio of the Intrinsic Specific Energies perpendicular to parallel at 50% RH is 52.7%.

is dried. The plywood should therefore be manufactured with as low a moisture content as is practical.

The standard deviations of the strengths of the custom made hexagonal birch plywood are considerably smaller than that of the commercially available conventional birch plywood. See Table 2. Furthermore, the samples cut from the same board have strengths that are grouped much closer together. This could indicate that there are significant differences in the material used in the construction or changes in the bonding procedures as to quantity of adhesive or its curing. The very low measurements came from boards which could probably be detected by use of non-destructive means such as flexural modulus measurements. This would leave the remainder of the boards with a standard deviation of less than 5%. These effects can be examined further in testing the remaining boards.

One unexpected factor in the results is that the strengths of crossply plywood tested parallel to the face grain was only 3% stronger than the same material tested perpendicular to the face grain at 50% RH, and actually 13% weaker after vacuum drying. This compares with a 25% increase in strength initially anticipated on the basis that the 9 ply material has 5 or 4 veneers parallel to the tensile stress direction respectively. This may be an artifact of small sample size, and should be clarified on further testing. Alternately it could be an inherent feature of plywood tests in that the material is gripped and stressed from the outer surfaces. This could cause the face veneers to fail sooner than the interior veneers when stressed parallel to the grain due to the higher stiffness compared with the cross-grain direction. A third possible cause could be in the application of high temperatures in hot pressing during manufacture. This might either degrade the material or cause poor bonding through premature pressure release.

In an attempt to identify the cause of these results, some birch plywood was specially ordered (18). The nominally half inch conventional 0°, 90° plywood was made up of 15 plies of 0.9 mm (1/28") veneers. Part of the boards were made using a cold-press urea adhesive with the balance made using a conventional hot press resorcinal adhesive. A larger number of samples was also planned. This material has been received and is available for future testing in subsequent programs.

This series of tensile tests and density measurements has provided some of the fundamental information on the distribution of strengths of plywood that is necessary to be able to use plywood in such an engineering application with a given confidence level. The broad distribution seen in conventional commercially available plywood was substantially reduced in custom-made clear hexagonal plywood. The strength of this hexagonal yellow birch plywood in the weakest region bisecting adjacent plies was also double that of the conventional crossply imported birch. Vacuum drying the plywood reduced the strengths on the order of 10% as was anticipated from trends observed in related literature.

While the general trend has been established, more data is needed to obtain more statistically accurate measures of the performance and changes. This is particularly important at the low strength end of the distribution where the design parameters must be set. More careful control is needed of the moisture and density measurements so that the intrinsic specific energy of the material can be evaluated. Otherwise the testing method and equipment has been developed, and further testing should proceed rapidly.

B. HIGH RESOLUTION TENSILE TESTING WITH ACOUSTIC EMISSION MEASUREMENTS

Conventional ramp or fatigue tensile tests typically produce data only on the stress at fracture or the duration of a stress cycle before fracture. Typically numerous lengthy tests must be performed over some length of time. This is particularly true if sufficiently accurate data is to be obtained to extrapolate results to the ultimate duration of load over the projected operating stress conditions. It would be useful if information on the rate of fracture as a function of stress could be obtained during short term tests. The ultimate strength and duration of load could presumably be inferred from such data.

There is some evidence in the literature which indicates that the rate of permanent deformation or damage increases rapidly when stressed above a given value which is approximately 50% of the short term strength (3). This is also the approximate stress level that is projected to be sustainable over 30 years or longer. If this level could be reliably measured in a short term test and be correlated with the long term strength, it would greatly simplify the efforts of measuring the useable strength for new species or moisture conditions.

The concept of a proportional limit as the beginning of major plastic deformation and material damage is widely used in metal testing. Such conventional analysis of load deformation curves is difficult to apply to wood since it exhibits considerable viscoelasticity. Any estimate of a proportional limit based on a given offset or graphical estimation by an operator is dependent on the rate at which the test was conducted and is not an inherent absolute material property. Furthermore, the nonlinearity in a typical tensile load-deformation graph is only on the order of 1%. Imaginative and painstaking tests have therefore been required to separate the effects of recoverable

viscoelastic response in the wood from irrecoverable viscous permanent deformation or creep. Some tests involve a cycle of loading and then unloading the material to determine the residual deformation. This is plotted as a function of stress to observe any rapid increase in the parameter. Ivanov, for instance, used a constant rate of loading and unloading to constantly increasing levels (23). The residual deformation at the bottom of each cycle was plotted against stress. Sugyama monitored the creep rate as a function of time for different stress levels (24). The creep rate after a given time was plotted versus stress and showed a break in the curve.

In other tests acoustic emissions occurring in the sample during a tensile test have been monitored. The rates of acoustic emissions also show a rapid increase after the stress reaches a certain level (25). Very few such tests have been made on wood (26). If the acoustic emissions are caused by failure of individual tracheids, this presumably indicates damage to the material. Furthermore the sample would become more flexible as well as weaker. If there were no viscoelastic deformation, the load deformation curve would presumably curve at higher stresses as the modulus of the material was reduced. The viscoelastic deformation may also increase more rapidly as a result. Accurate analysis of the slope of the load deformation curve may therefore reveal a rapidly changing rate of curvature above a certain stress region.

It was therefore proposed to conduct an exploratory study of the nonlinearity of the load deformation curve coupled with monitoring the acoustic emissions. These would be compared with the stress and the long term durability to see if some correlation could be made.

Examining the system using a first order analysis, the spring constant of the sample can be considered as made up of a series of groups of fibers in parallel. The change of the overall spring constant is thus related to the

fracture of the component fibers. The acoustic energy released when those fibers are broken is proportional to the stiffness of the fibers times the square of the strain at failure. If the fibers are hypothesized to fail at equal strains, then the acoustic energy released should be proportional to the stiffness of the fibers broken. The power present in the acoustic emission signal being monitored by an ultrasonic sensor is proportional to the square of the signal. Ignoring side effects, nonlinearities, damping, resonances, etc., it is hypothesized that the integration of the square of the acoustic emission signal will be proportional to the change in stiffness or modulus of the tensile sample during the test. (See Figure 21.) Both are expected to increase more rapidly with stress above a given stress region which could correlate with the long term strength. High resolution measurements of the load deformation curve coupled with the acoustic emissions were therefore proposed. The equipment to perform these tests was specified or designed and procured or built as follows. (See Figure 21.)

B.1. Equipment

The combined requirements of high resolution, accuracy and speed in sampling data during a standard tensile test precludes taking data by conventional chart recorder or by hand. Therefore, a micro-computer based data acquisition system was chosen to monitor and record the data, and to provide the preliminary data manipulation and reduction. The curvature seen in conventional tensile tests is on the order of 1-2%, part of which is due to the recording equipment. In order to resolve the nonlinear effects to the 1% level, an equipment precision and accuracy of 0.01% was chosen. This is considerably more stringent than most equipment available for stress and strain measurements.

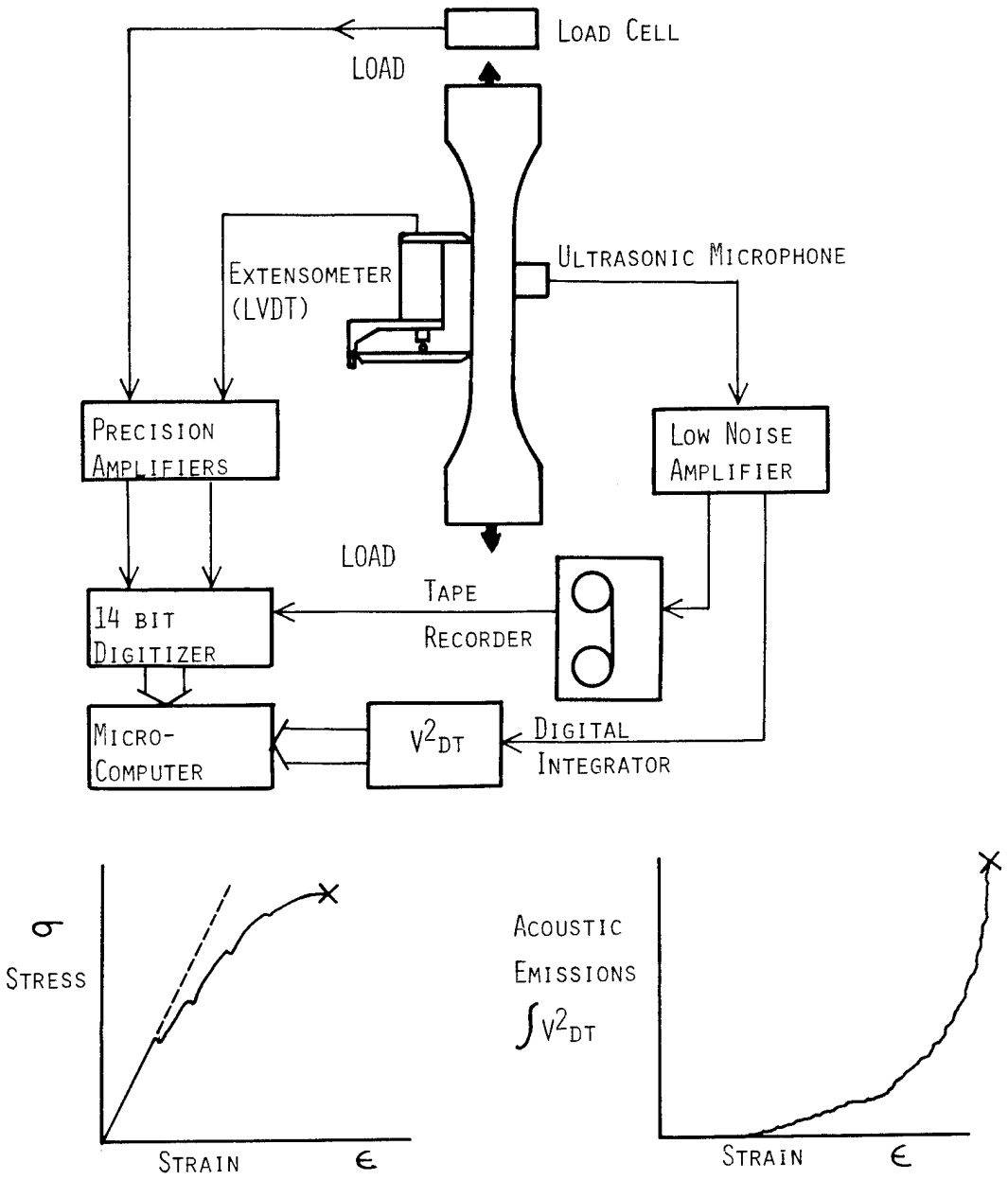

Figure 21. High Resolution Plywood Tensile and Acoustic Emission Tests at University of Minnesota, 1979

Microcomputer -- Obtaining data with 0.01% resolution requires 14 bit binary data to be measured and recorded (1 part in 16,384). Microcomputers with 8 bit words would require two words per number, making data handling awkward and slow. Therefore, a microcomputer with 16 bit words was chosen. Fortunately there are a large number of Digital Equipment Corporation PDP 11-family computers at the University of Minnesota including a rapidly growing number of Teraks which utilize DEC's LSI-11 microprocessor. Digital Equipment Corporation's PDP 11-03 with this LSI-11 was therefore chosen and obtained from a local company which offered us an unused system (for this project) substantially below the list price.

Digitizer -- Most digitizers currently on the market only have a resolution of 12 bits, which would be insufficient for the goal of 0.01% resolution. A sixteen channel multiplexed 14 bit digitizer board #1014 was located and obtained from the ADAC Corporation. This is a dual width board which slides into the PDP 11-03 backplane.

Real Time Clock -- To provide an accurate time base to trigger the measurements, a real time clock #8T2769 on a dual-width board was obtained from Data Translation Inc.

Patch Panel -- Unwanted noise in the lines becomes significant when working at 14 bit resolution (0.5 mV in 10V). Therefore the connecting cables were made from two conductor shielded cable with three pin amphenol connectors which are commonly used in audio systems. A sixteen channel patch panel with these receptacles was constructed to connect the signals to the A/D board.

Instrumentation Amplifiers -- The digitizers require a 10V full scale signal while load cells typically provide a signal on the millivolt level. Instrumentation amplifiers of the required accuracy, stability, and nonlinearity were not found at an acceptable price. Therefore instrumentation amplifier modules

#606J from Analogue Devices were obtained. These were mounted on printed circuit boards along with the gain resistors and trim pots. The gain resistors were 0.1% with 25 ppm temperature coefficient. Each resistor was connected to a trim pot to be able to adjust it to within 0.01%. Since the data was being recorded in octal format, a binary sequence of gain resistors was chosen ranging from 2^0 to 2^{14}. The printed circuit boards were mounted on a panel containing the input/output and zero reference connectors along with the gain switch. A null trimming pot and a signal reversing switch were also provided on the front panel along with a zero-offset reference voltage switch. The latter was provided with octal division of $\pm$ 10V and connected to a Dekapot or pair of potentiometers in series placed on an adjacent panel.

Reference Potential -- A $\pm$ 10V reference voltage was provided with the power supply to the rear bus of the amplifier panel. The reference lines were provided with Darlington transistors to provide sufficient current to drive the load cells. They were also divided through a four stage octal divider to provide a simple means of changing ranges in the reference offset as well as the gain.

Extensometer - The extensometer available had a number of linkages and pivots moved by gravity. Some difficulty was experienced operating this equipment as well as there being uncertainty as to its accuracy and linearity. A simple extensometer was therefore designed which had only one knife edge pivot and in which the core of the LVDT was spring actuated. The unit was supported by knife edges to the sample. A gage block between the two knife edges would be used to provide the initial positioning. The wood samples strain approximately 1% at failure. With a 50 mm (2 inch) gage length the total travel of the extensometer would be 0.5 mm (0.02 in). An ultra precision LVDT was therefore ordered from Schaevitz Engineering which had a nominal range of $\pm$ 0.050 in.

It has a nominal nonlinearity of 0.1% which could be calibrated and accounted for later.

Programs - An assembly language program has been written to acquire and record the data. This program can specify the channel number, order and frequency with which the data is to be taken. The stress and strain data are alternately taken and then averaged every sixteen points. This helps remove noise and improve the resolution four times to give full 16 bit significance to the data, assuming major effects do not occur within this time. Using this approach, 200 pairs of averaged points can be recorded on floppy disk each second. Over a five minute run, this would result in 60,000 pairs of points. To measure the slope, a least squares fit will be made every hundred points for instance. Alternately, deviations from the initial slope could be portrayed. Periodically a set of reference points will be monitored. These would provide a check on the drift of the amplifiers and reference voltages. The temperature of the sample could similarly be monitored. The program also provides a visual monitor of the progress of the test by displaying it on the CRT when used with a TERAK microcomputer.

Load Cells - The load cells that are available with the Instron testing equipment in the Forestry Department are over 15 years old and are only specified to 0.1%. Although it may be possible to calibrate these, it will be necessary to purchase a high accuracy load cell if the hysteresis and drift are too great. (Such cells with 0.01% nonlinearity are available from Interface, Inc.)

Acoustic Emissions: Sensors - Early tests of acoustic emissions of wood used simple accelerometers, and all information above 7 kHz was filtered out.(25) More recently conventional ultrasonic acoustic emission apparatus was applied to test finger joints.(26) In this case all information below 125 kHz was filtered out. Some information existed above this though a frequency power-analysis indicated that most of the information was below this point. Little

exists in the way of sensors to monitor emissions in the range from 10 kHz to 100 kHz with the sensitivity desired for such testing. Piezoelectric crystals with a resonance at 65 kHz were therefore obtained. These will be complemented with conventional accelerometers which typically have a resonance around 30 kHz and with some low frequency ultrasonic sensors with a resonance at 125 kHz. The National Bureau of Standards is currently developing absolute calibration methods for use in the conventional ultrasonic range from 100 kHz to 1 MHz. These may be extended down to the range of interest here.

To record the acoustic emissions, some instrumentation tape recorders (CDC PR3300 made in 1963) were obtained through Sandia Labs from equipment placed on the Federal surplus equipment list. These recorders have a nominal bandwidth up to 100 kHz in the direct-record mode at 60 ips. They can also be operated at 1 7/8 ips by changing belts. It was planned to record that data at full speed and then play it back at the slowest speed to digitize it with the available digitizers in the data logging equipment. However, when the recorders arrived, they only had the high speed belt set. New belts were quoted by Bell and Howell as requiring six months to deliver. Furthermore, the signal to noise ratio was 35 dB at best under signal condition.

To bypass these difficulties, a high speed digital integrating circuit was designed, and the parts ordered. A high speed sample-and-hold chip and a 12 bit digitizing chip were ordered to digitize the acoustic emission signal with a throughput of 500 kHz. This corresponds to a 65 dB signal-to-noise ratio indicating that the limiting factor will probably be noise in the sensors and amplifiers. If the data is taken at a constant rate and summed, it will essentially provide a digital integration of the signal. A TRW#TDC 1010J chip that can multiply and accumulate two 16 bit numbers in a tenth of

a microsecond was ordered. By feeding the digitized signal at a constant rate to both inputs, the chip squares-and-integrates the signal. The output is then shifted to obtain the most significant 16 bits of the 32 in an output register that can then be read via the microcomputer via a parallel input port. All the chips have been acquired except the sample-and-hold and digitizer. The order for these was misplaced during a company merger delaying the chips delivery three months. In the meantime, belts for the recorders were obtained on loan from another surplus house in California. These will enable the acoustic emission signal to be recorded and played back at slower speed as originally planned. This will prove valuable to permit a frequency analysis of the signal, thereby clarifying the region from 7 kHz to 100 kHz which has not been monitored before. Sensors with appropriate resonance can then be chosen to match the sensors maximum sensitivity to the strongest frequency of the signal.

Resolution and sensitivity in much acoustic emission research have been limited by noise transmitted from the machine through the grips or directly through the air. Noise from the test equipment has been effectively eliminated by introducing an acoustic isolator consisting of multiple layers of metal and polymer in between the machine and the grips.(27) Wedge grips incorporating this principle were therefore designed. On reviewing the original design, it was realized that they would crush the sample. The wedge angle must be increased from that existing on commercial grips. Anechoic foam was obtained to line the inside of the environmental box that fits the Instron test equipment. This should reduce the amount of room noise being picked up by the sensors.

The instrumentation amplifiers have been built and calibrated. The equipment and programs are therefore ready to begin monitoring the load and deformation, and the acoustic emissions can be recorded by the tape

recorders. Time limitations precluded any further measurements in this task. These can be made in subsequent programs with little further effort. The acoustic emission measurements could be considerably improved as soon as the digital integration equipment and the acoustically isolated wedge grips are made.

Thus the equipment needed for high resolution data acquisition using a microprocessor has been obtained. Equipment was also designed and the parts ordered to monitor and digitally integrate acoustic emission signals up to 100 kHz which should give unparalleled performance. Measurement of the load, deformation and acoustic emissions to this accuracy and resolution should enable future measurements of the change in elasticity and damage rates in tensile samples. This unprecedented capability could be applied to Kevlar, fiberglass and other composites as well as wood, opening up a new realm of durability measurements.

C. TENSILE FATIGUE TESTS OF PLYWOOD

A typical stationary flywheel energy storage system may be designed for a life of 30 years of diurnal cycling or 10,000 cycles. The cyclic nature of the stress affects the durability of the rotor through fatigue. The actual nature of the effects, however, is not clear from data existing in the literature, particularly for vacuum dried plywood.

Conventional fatigue tests of wood on a rapid cyclic fatigue machine have been performed and show that wood is quite durable.(28,29) The damping or internal friction results in considerable heating in the sample. This is significant since wood as a viscoelastic material exhibits a creep rate that is exponentially proportional to the absolute temperature. The creep under constant stress also degrades the material. Constant creep has been shown to be more detrimental than daily applying and removing the stress up to

several hundred cycles.(24) This indicates that the duration under stress may be more significant.

This concept has been developed recently in the form of several damage theories.(30,31) These theories use a relation between the stress and the damage rate and integrate it over the expected stress history. To obtain data as to the effects of fatigue and stress on vacuum dried plywood, it was proposed to study such fatigue on an available cyclic fatigue machine. Comparable tests would be run at ambient conditions to compare the results with other studies. Four or five decades of time could reasonably be tested on such a machine if stresses were chosen to give mean times to failure of 0.1 hr (6 min), 1 hr, 10 hrs, and 100 hrs (4 days). These could be compared with the ramp tests on the Instron which could be performed in 0.01 hr (0.5 min). To simulate a speed ratio of 1:3, a fluctuating load would be chosen so that the minimum to maximum load ratio is 1:9.

A pseudoisotropic cellulosic rotor will probably use a hexagonal assembly where the veneer directions are 0°, 60°, and -60°. The weakest region of the plywood is probably the region bisecting the grain direction in adjacent plies, i.e., perpendicular to the face grain where the angle to the veneers is 90°, 30°, and -30°, respectively. Due to the length of the tests, it was decided to concentrate initially on this direction using the vacuum dried custom made hexagonal birch plywood. The samples to be tested in tensile fatigue are identical to those used in the ramp tensile tests. The testing must be done in a controlled atmosphere of dry nitrogen or 50% RH.

Equipment - The cyclic fatigue test machine available to the project was developed by B. J. Lazan at Syracuse University and is one of a number fabricated and used by the Aeronautical Engineering Department at the University of Minnesota.(32) (See Figure 22.) The machine uses an adjustable eccentric weight driven by a synchronous electric motor at 3600 rpm (60 Hz) to produce

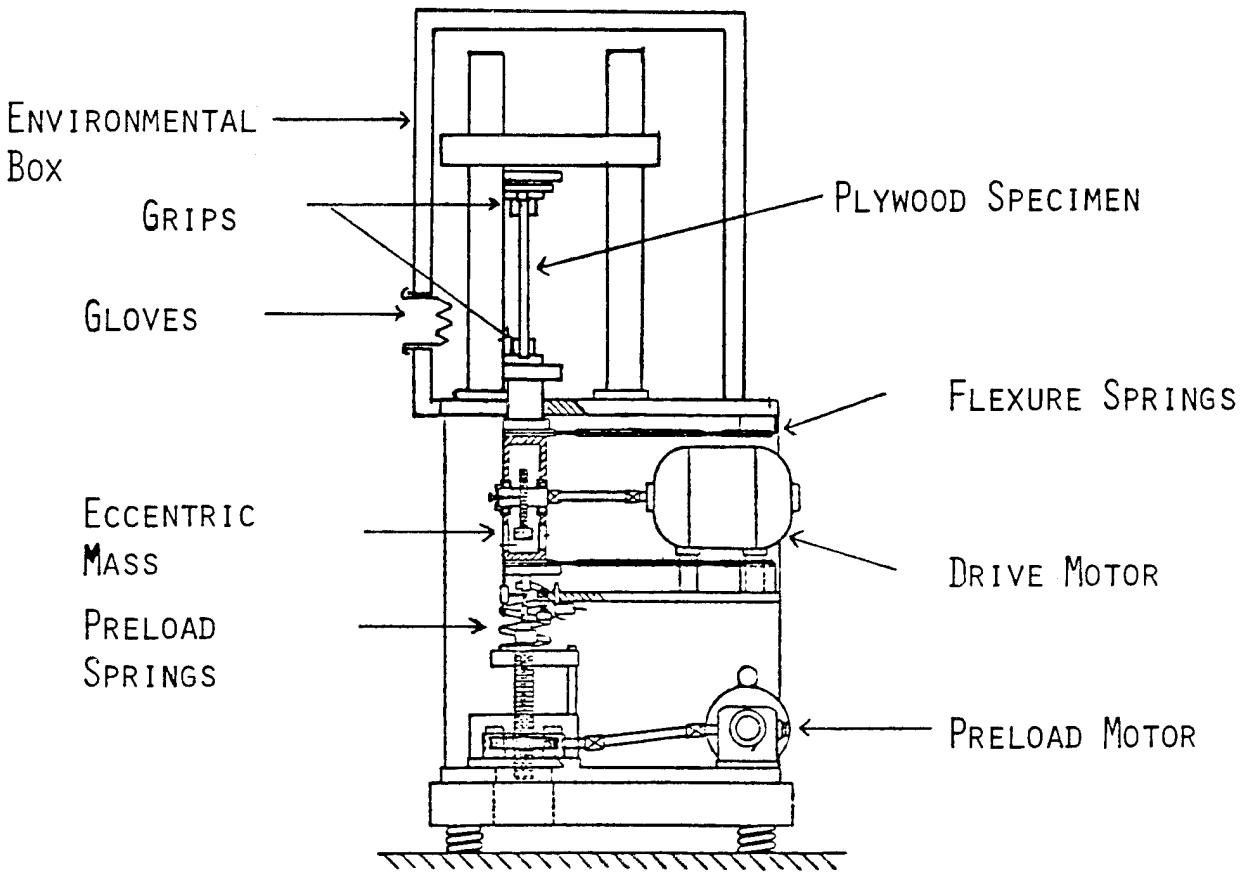

Figure 22. Syracuse Dynamic Creep and Fatigue Testing Machine @ University of Minnesota

a fluctuating load. A pair of springs is used to maintain a tensile preload on the sample.

The machine automatically maintains the preset preload-spring extension by lowering the bottom spring support in the advent of extension of the sample due to elasticity or creep. Failure of the sample causes the eccentric cage to contact a micro switch which shuts off the power and applies a brake.

The load applied to the sample was described as:

$$F_{mx} = F_p + F_a$$

$$F_{av} = F_p$$

$$F_{mn} = F_p - F_a$$

where F_{mx} = maximum load applied

F_{av} = average load applied

F_{mn} = minimum load applied

F_p = spring preload

F_a = alternating eccentric force

These equations hold for relatively stiff materials such as steel or aluminum which have a Young's modulus E in the range of 71 - 210 GPa (10-30 Mpsi). Birch plywood by comparison has an modulus on the order of 3.5 GPa (0.5 Mpsi), which complicates the equations. The flexibility of the wood requires two corrections:

1) The fluctuating load causes a significant displacement of the eccentric cage. At the bottom and top of the cycle these displacements are in series with the preload spring, changing the load they apply. The mechanism which maintains the constant spring extension will cause the maximum load to remain at $F_{mx} = F_p + F_a$, but the average and minimum loads F_{av} and F_{mn} will have different values.

2) The flexibility of the wood drastically lowers the spring constant of the system and therefore lowers the natural resonance frequency of the spring mass system. Initial calculations have shown a natural frequency

of approximately 80 Hz compared to a driving frequency of 60 Hz, resulting in a transmissibility significantly greater than unity. The actual transmissibility depends on the spring constant and damping coefficient of the particular sample being tested.

The corrected load equations resulting from including these effects are as follows. (The derivations are shown in the Appendix)

They are:

$$F_{mx} = F_p + F_a$$

$$F_{av} = F_p + K_s X_a$$

$$F_{mn} = F_p + (K_s - K_w) X_a$$

where the maximum alternating cage displacement X_a is given by

$$X_a = T_m (F_a / K_s + K_w)$$

T_m = motion transmissibility = $\frac{\text{Actual Displacement}}{\text{Static Displacement}}$

K_w = spring constant of wood sample N/m (lbsf /in)

K_s = spring constant of preload springs N/m (lbsf /in)

The eccentric is adjusted to give an alternating force relative to the maximum and minimum forces as given by:

$$F_a = \left(T_m \frac{(K_w - K_s)}{(K_s + K_w)} + 1 \right)^{-1} \cdot (F_{mx} - F_{mn})$$

Similarly the preload spring extension is set so that:

$$F_p = F_{mx} - F_a$$

As seen from the preceding equations the parameters K_s, K_w, must be determined to set the test loadings.

The preload spring constant K_s was readily measured by placing a load cell in the machine in place of a sample and measuring the load at several

preload-spring extension settings.

The spring constant K_w varies between samples as static tensile tests have shown.

To obtain accurate fatigue data, K_w would have to be evaluated for each sample.

In testing a number of samples to obtain K_w, it was found that a number of extension-relaxation cycles were necessary before the spring constant would approach a steady value. The sample stiffnesses K_w from the initial few cycles were found to be 8% lower than the following cycles. The stiffness of the wood may also change during the course of a fatigue test.

The motion transmissibility T_m is dependent on the eccentric speed (ω), natural frequency (ω_n) and the critical damping ratio ζ. i.e.,

$$T_m = \frac{1}{\left\{\left(1 - \frac{\omega^2}{\omega_n{}^2}\right)^2 + \left(2\zeta \frac{\omega}{\omega_n}\right)^2\right\}^{\frac{1}{2}}}$$

Natural frequency is dependent on the mass (M) of the eccentric cage and attached fixtures and the combined spring constant of the system $K_s + K_w$, $\omega_n = \sqrt{(K_s + K_w)/M}$.

The eccentric speed is a constant 60 Hz (3600 rpm). The critical damping ratio is equal to the ratio of damping coefficient b and the critical damping coefficient b_c where $b_c = 2\sqrt{(K_s + K_w)M}$.

To find the transmissibility either the natural frequency and critical damping ratio must be determined or the displacement at a known cycle load must be measured. The natural frequency calculation requires an accurate measurement of the mass. Direct measurement of the cage mass would require disassembly of the machine, and the results would still be questionable because of the mass effects of the springs. The mass of the cage was

calculated from volume measurements to be 14.6 kg (1.0 slug). Together with the spring constants of K_w = 3.5 MN/m (20,000 lb f/in) K_s = 0.18 MN/m (1040 lb f/in) this yields a natural frequency of 80 Hz. The natural frequency of the cage-spring system was measured by providing an impulse (hammer tap) and noting the resulting motion. The vibrations had a frequency of 85 Hz to 87 Hz which is in reasonable agreement with the 80 Hz estimated from the mass and spring constants.

With ω/ω_n = 60 Hz/80 Hz, = .75, Figure 23 shows that $2.3 > T_m > 2.0$. Assuming a critical damping ratio of $\zeta > .2$. To confirm this value, measurements were made on the cage displacement with a traveling telescopic on a venier stand, while the cage's image was frozen at different points with an adjustable strobe light. The telescopic measurements gave a T_m between 1.1 and 1.3. To complement these measurements, an accelerometer was placed on the cage. This showed peak accelerations of 4 g's at a 200 lbf fluctuating load, which at a frequency of 60 Hz, represents a transmissibility of 1.14, see Figure 23.

Both these measurements of T_m are well below the values estimated from the relative speed and damping. The presence of a critical damping ratio greater than .2 might explain the discrepancy. However, telescopic measurements to determine the motion of the cage with respect to the eccentric showed a phase angle of less than fifteen degrees. This would indicate that ζ is less than .1, not enough damping to account for the lowered transmissibility.

These measurements indicate the difficulty in calibrating this equipment when it is used with plywood samples with low stiffness. Furthermore, such a calibration is not absolute, but varies with the stiffness of the sample which could change during the test.

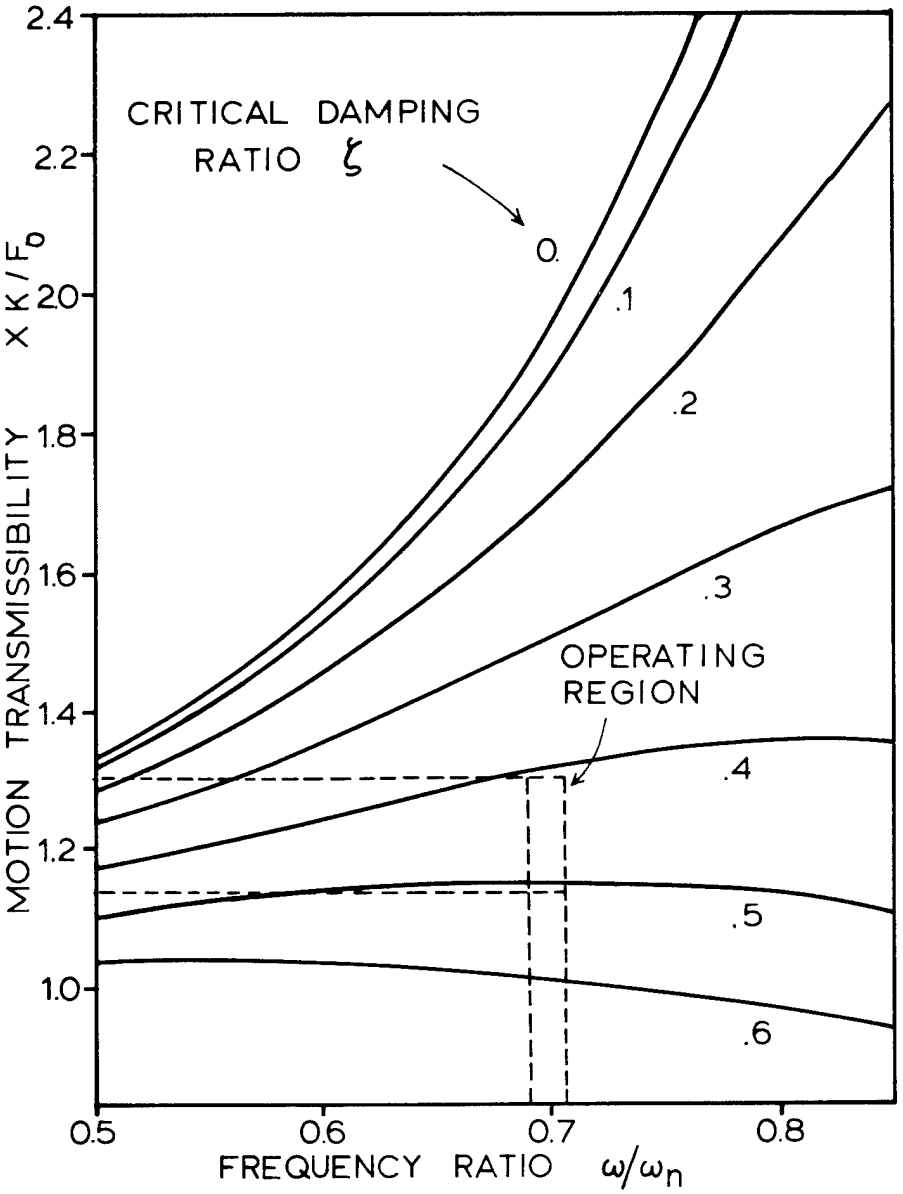

Figure 23. Eccentric Cage Motion With Plywood Specimen

Because of the accuracy problems in the calibration of the machine shown above we believe a load cell must be installed in the head of the machine to measure precisely the loads developed. Such a fatigue-rated load cell could be installed with some modifications to the machine in future testing. Such fatigue testing would still be necessary to compare with the high resolution tensile experiments.

D. ROTOR-HUB FATIGUE

Of fundamental concern in designing flywheels is the long term durablility of the rotor-hub system under the projected operating conditions. Tensile fatigue strength measurements of the rotor material are needed to provide information on the expected performance of the rotor. However, such tests cannot precisely duplicate the stresses experienced by the rotor during its operation. This is particularly true of pseudoisotropic rotors where there is a continuously varying complex combination of biaxial tension and shear within the rotor. Of particular concern are the stresses near the hub, where the power torque and imbalance moment in the system are also applied.

Cyclic Rotor-Fatigue Experiment - A cyclic rotor-fatigue experiment was originally proposed to test the durability of light rotors under actual operating conditions. The original concept proposed, was to cycle two rotors by transferring the energy from one to the other through a Continuously Variable Transmission (CVT), i.e., one rotor would be brought up to speed independently with a motor. The input-output ratio of the CVT would then be gradually changed, decelerating the first rotor and accelerating the second until the minimum speed of the first had been obtained. The second rotor would then be at its maximum speed less the

inefficiency in the CVT and connected components. The second rotor could then be brought up to its full speed with the motor. This system is conservative of power, highly efficient, and would have the advantages of cycling two rotors simultaneously.

A detailed design for such a cyclic rotor-fatigue facility was made during the Fall Quarter of 1978 together with six seniors and a graduate student in the Design Division. (33) Over five hundred man-hours of effort went into the design and detailed drawings. The apparatus designed is shown in Figure 24. The design is centered around a 10 kW (13 hp) Kopp Variator CVT mounted in a vertical configuration between two rotors. Each rotor was provided with the appropriate vacuum container and burst containment. The power transmission train was provided with torque isolators and clutches to protect the CVT. An electromagnetic-clutch and motor were provided to power the system. A cyclonic filter was provided to exclude from the vacuum pumps any fragments that might escape the burst containers.

A large pressure tank was located as a possible lower container. This was designed larger than the upper container with a view for providing room for a large full scale rotor. A large vacuum pumping system consisting of a Rootes Blower backed up by a roughing pump was acquired on loan from another department. This could handle the amounts of water potentially anticipated from wood rotors. There was some indication that the CVT would be donated to the project. A more detailed estimate was made of the cost of constructing and installing the system based on the design drawings completed.

Upon reviewing the design, the projected costs, time and personnel requirements with the project administrators, it was decided that there were insufficient funds for such a project, and that it required considerably more time and effort than were available considering the other project

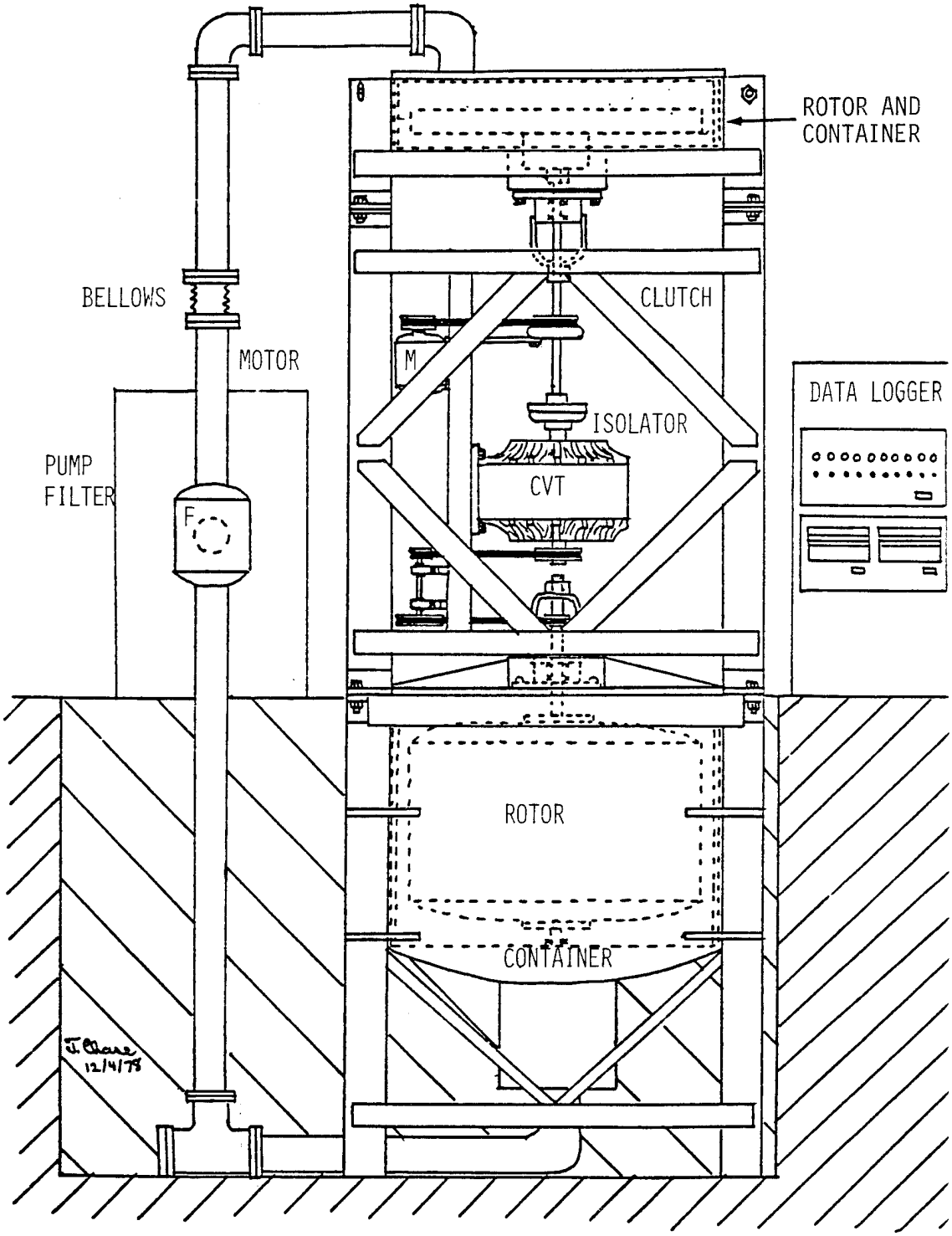

Figure 24. Dynamic Dual Rotor Fatigue Apparatus

tasks. Furthermore, it was found that the vertical axis Kopp Variator was not readily available though designs for it did exist. For future consideration, therefore, the design for the CVT should be modified to a horizontal configuration as shown in Figure 25. This configuration would provide the advantage that the vacuum/burst containers could both be underground, providing greater safety. This would require two additional right-angle gears which could be used to step up the CVT shaft speed. The original design would have accommodated full 1.5 m (5 ft) wide rotors which are potentially possible considering the 1.5 m square birch plywood commercially available from Europe. This could be reduced by half to reduce the vacuum-container assembly and installation costs while still providing credible rotor tests.

Pseudo Cyclic Rotor Fatigue Experiment - In re-evaluating the project and the original goals, it was concluded that the primary requirement was to obtain data on the durability of the hub-to-rotor bond. To obtain such information, it was decided to attempt to modify an existing flexural fatigue apparatus to simulate the combined effects of the imbalance moment on the hub together with the cyclic torque due to accelerating and decelerating the rotor. The major disadvantages of this approach is that it does not include the effects of the rotary stresses induced in the rotor.

The schematic design for the dual-mode fatigue apparatus is shown in Figure 26. The effect of imbalance in the rotor is to apply a moment to the shaft in the plane of the imbalance (assuming the rotor is spinning considerably above or below the fundamental transverse resonance speed). This is potentially the greatest cause of failure next to the rotary stresses. The cyclic torque is applied by connecting an electrically driven rotating weight to a lever arm attached to the tube connected to the hub. Lever arms were used to multiply the applied forces for both

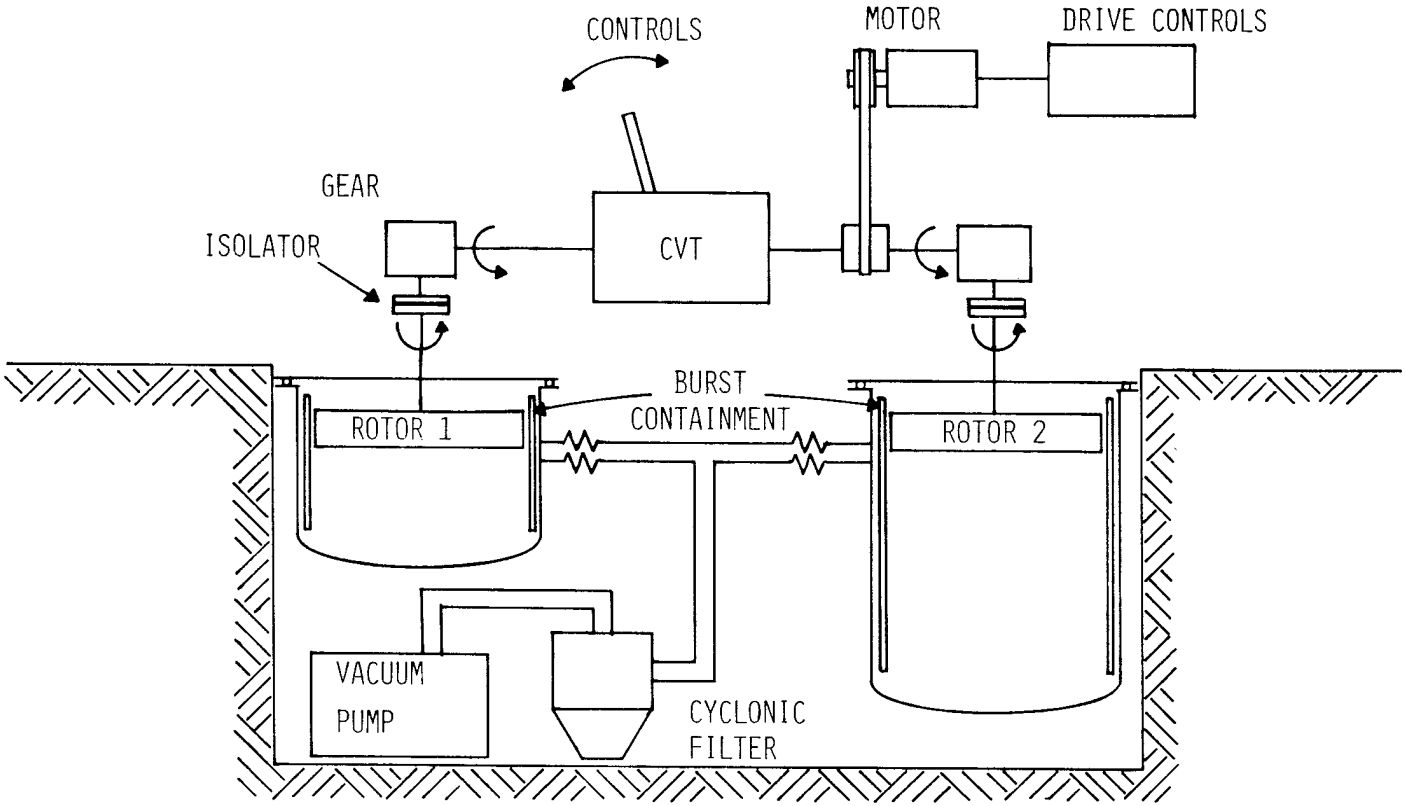

Figure 25. Modified Dynamic Dual Rotor Fatigue Apparatus

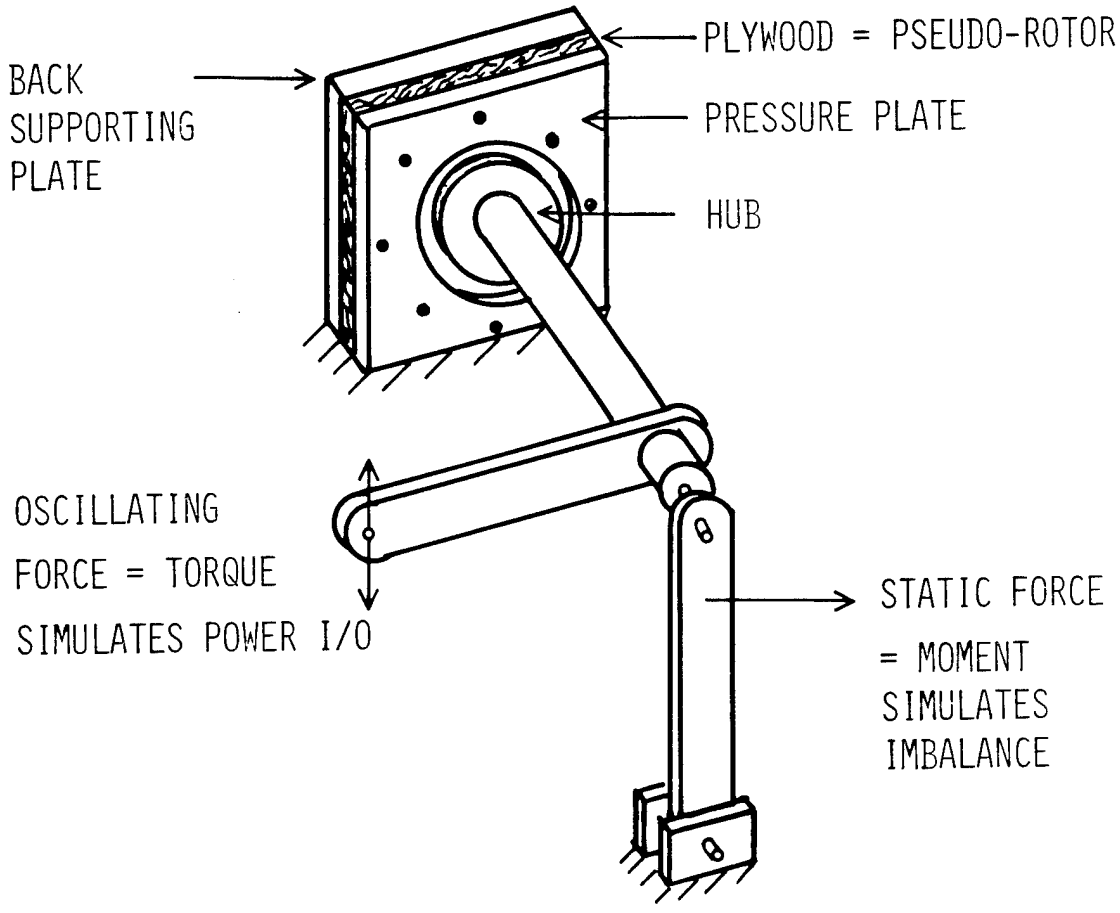

Figure 26. Hub-Rotor Bond Fatigue Apparatus, University of Minnesota, 1979

the moment and torque to enable reasonably sized weights to be used. The torque that can be transmitted by a hub of radius R_p is: $T = \pi\tau R_p^3/2$ = 479 τNm (42.4 τ in-lbs) where the maximum shear stress allowed τ is given in kPa (psi) for the 12 mm (6") diameter hub in question. Even with a nominal 276 kPa (40 psi) applied shear stress, the hub could transmit 191 kNm (141 ft-lbs). At a rotational speed of 523 rad/sec (5,000 rpm), this results in a power transmission capability of 100 kW (134 hp). Typical residential applications require only one tenth of this. Thus the design can be left very conservative or the hub could be reduced in diameter.

A 300 mm (12") diameter plywood disk is bolted between 19 mm (0.75") steel plates. The front plate has a 250 mm (10") hole cut in it to allow strains to develop around the hub while still rigidly clamping the plywood. Hub plates 153 mm (6") in diameter and 12 mm (0.5") thick are attached to the plywood according to the hub-to-rotor attachment method being tested. This is then bolted onto a corresponding disk to which is applied the torque and moment. LVDT extensometers are connected to the ends of the moment and torque arms to monitor the strains and creep which are magnified by the relative lengths.

The apparatus has been constructed and a few hub-rotor combinations tested to check out the machine. Detailed testing on this equipment could be performed during subsequent programs.

E. ROTOR DRYING RATES AND METHODS

The hygroscopic nature of cellulose and its shrinkage or swelling with moisture changes is a fundamental property that must be taken into consideration when assembling such rotors. If the disks are equilibrated at ambient conditions of around 50% relative humidity, the material will contain around 8% to 10% moisture content. If the disks are bonded into

a rotor and then placed in a vacuum, the outer surfaces will dry rapidly and shrink. It will take quite some time for the moisture in the center of the rotor to diffuse out. This results in the outer surface material shrinking much faster than the center causing the plies to separate around the edges.

To solve this dual problem of splitting due to unequal shrinkage, and of the long time required to dry a large rotor, it is necessary to dry the disks before they are assembled into a rotor. Similarly the veneers must be dried as much as practical and adhesive chosen for minimum moisture content when the thin disk material is assembled.

The corollary of this splitting problem, is that if a dry disk is placed in a humid environment, it will rapidly absorb moisture on the outside which will swell, causing the plies to separate in the interior. A dry rotor must therefore be kept dry. One approach to this problem is to coat the rotor with a hermetic epoxy coat such as has been developed by boat builders. (10) Such a coat may also be useful in minimizing the rate of removal of moisture or volatile chemicals from the rotor while in a vacuum. This could minimize the pumping requirements and possibly permit periodic pumpdowns if hermetic rotor containment is desirable.

The rate at which moisture can be removed from a rotor or disk affects the pumping requirements and the drying costs. Moisture loss has been assumed Fickian or gradient dependent by most reports in the literature. (34) There is some controversy as to whether the diffusion is dependent on the moisture content or vapor pressure gradients and if this is valid for bound water. (35) Some preliminary data from one experiment showing the rate of moisture gain of a vacuum dried plywood cylinder when subjected

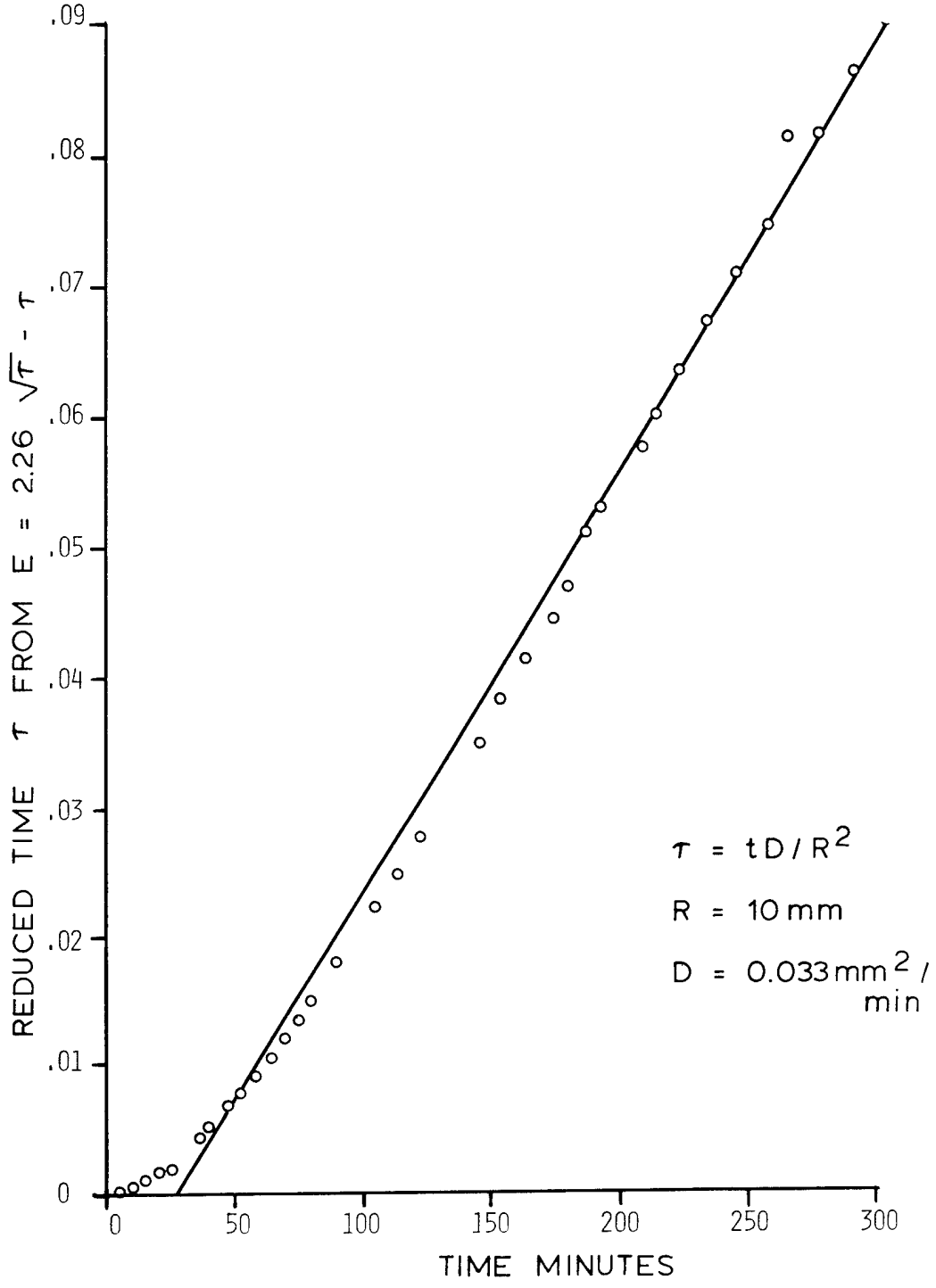

Figure 27. Humidification of Vacuum Dried Plywood Disks

to a moisture saturated environment is shown in Figure 27. An approximate relation which is valid for short times ($\tau < 0.2$) for the fractional change of moisture content $\bar{E}$ (relative to the final asymptotic change) is:

$$\bar{E} = 2.26 \sqrt{\tau} - \tau$$

where the reduced time τ is given by

$$\tau = tD/R^2$$

for time t, diffusion coefficient D, and cylinder radius R. Fitting the data to this equation gives a diffusion coefficient D of .033 mm^2/min.

The corresponding general equation is:

$$\bar{E} = 1.0 - \frac{1.60}{\exp(5.76\tau)} + \frac{1.07}{\exp(30.6\tau)}$$

Further detailed measurements are needed of the diffusion coefficients and to check the validity of these equations for vacuum drying of cylinders of finite length. Similar studies are needed of the effects of shrinkage or expansion during moisture changes, and of coating the rotors with epoxy sealants.

CONCLUSIONS AND RECOMMENDATIONS

The scalloped band hub-rotor attachment designed appears to be potentially more durable and have less damping than the elastomeric interface method of attaching hub to rotor. A parametric and experimental study of this system should be made to evaluate the effective vibrational characteristics and durability of this design.

The alignment-type balancing methods appear promising for high performance pseudoisotropic rotors, as well as wound rotors, in eliminating the need to add or remove mass. The self-centering dynamic balancing apparatus designed should be easily constructed. Its capabilities and sensitivities should be further explored.

The economics of cellulosic rotors are very sensitive to rotor design. Rotors made of superpaper wound around a Tanguile plywood core appear to be competitive with similar rotors made of steel hose wire, particularly at lower container costs. Further comparisons of these two systems should be made with commercially realistic costs of containers and rotor assembly. This sensitivity similarly suggests that the comparative economics of containers and plywood rotors or cores should be re-examined as a function of the densities and strengths achievable by compressing them during manufacture.

Measurement of the drying rates of plywood disks and rotors appears straightforward with the appropriate equipment, based on preliminary measurements of miniature samples. Such drying rates and the consequent outgassing should be quantified to evaluate the costs and pumping requirements involved. The observation of warping of hexagonal plywood strips on drying (which is not observable with symmetric conventional plywood) suggest that internal drying stresses may be significant and should be examined further. Plywood for rotors should therefore be assembled as dry as possible and stored in a dry atmosphere.

The tensile tests performed provide initial data on the statistical distribution of the material properties that is necessary for cellulosic materials to be used as engineering materials. Commercially available birch plywood could be used for rotor cores, but has a large distribution of strengths. Careful quality control, combined with material screening using nondestructive methods, are needed to narrow the broad distribution of strengths seen. Some reduction in strength was noted on vacuum drying, comparable to the standard deviation of the strengths measured.

Hexagonal yellow birch plywood custom made commercially, demonstrated narrower property distributions (7-14%) and double the effective strength in the region bisecting the grain direction of adjacent plies. Rotors of

such plywood appear feasible. There is some correlation between the density of the material and its strength. Thus the intrinsic specific energy (strength to density ratio) shows a narrower distribution than the strength alone, and is the critical design parameter to be defined.

Proof-testing materials to above the use requirement should be used to verify rotor performance and eliminate the inevitable lower portion of strengths. The most economical design level and proof test level should be made a subject of further study. Lower cost materials with comparable performance and fewer defects (such as Tanguile) should be studied along with assembly-line production techniques to improve the economics.

Attempts to calibrate the cyclic fatigue apparatus when testing plywood samples indicated that each sample would have to be individually calibrated through a number of cycles to quantify the transmissibility of the equipment. Furthermore, this may change during the test beyond the limits required to obtain statistically valid data. Load cells and extensometers need to be added to the equipment to permit quantitative testing. The temperature of the sample should be monitored and the results compared with constant load fatigue tests.

The pseudo rotary-dynamic rotor-hub fatigue testing equipment designed will be ready for use after a few minor modifications are made. The dynamic rotary cyclic fatigue equipment designed to test two rotors simultaneously could be readily modified to use a horizontal transmission with the two vertical axis containers placed below ground. This modified design should be considered in the future for testing of prototype rotors when they are sufficiently developed for operational testing.

ACKNOWLEDGEMENTS

The authors would like to acknowledge the contributions made to this study by the numerous individuals and institutions who have worked with or discussed the project with us. Harold Schildknecht has been very encouraging and patient with us in overseeing this project for Sandia Laboratories. Scott Gaff and Alan Ost have worked hard at designing, constructing, calibrating and operating the tensile and fatigue test programs. Tom Chase and the other senior design students designed a very creditable cyclic rotary fatigue apparatus. Tom Chase and Sharadkumar Shah designed and constructed the pseudorotary hub fatigue experiment. Mike Gilbertson, Frank Kelso and Dave Fritz worked out the detailed design of the self-centering balancing apparatus. Shardad Tabib and Greg Stenberg designed and built the high performance amplifiers. Stuart Levy volunteered a detailed comprehensive computer program to log and analyze the experimental high resolution tensile test data. David Fritz and Frank Kelso contributed the rotor transmissibility apparatus and data.

The Forestry Department kindly provided the tensile testing facilities and loan of humidity control equipment. The Eaton Corporation provided technical assistance on their continuously variable drives. David Rabenhorst continued to provide encouragement and inspiration in pursuing these studies. Mike Gilbertson and Cathy Hagen drew the figures, and Lana Schermerhorn typed the reports.

Support for this program was provided by the U.S. Department of Energy as part of the Solar Mechanical Energy Storage Project work administered by Sandia Laboratories.

REFERENCES

1. Rabenhorst, D. W., "The Applicability of Wood Technology to Kinetic Energy Storage", Johns Hopkins University, Applied Physics Laboratory, APL/JHU Technical Digest, Vol. II, No. 5, May/June 1972, pp. 2-12.

2. Hagen, D. L. and Erdman, A. G., "Flywheels for Energy Storage: A Review with Bibliography", Design Engineering Technical Conference, Montreal, ASME Paper No. 76-DET-96 (September 26-29, 1976).

3. Hagen, D. L., "The Properties of Natural Cellulosic Materials Pertaining to Flywheel Kinetic Energy Storage Applications", Proc. 1977 Flywheel Technology Symposium, October 5-7, 1977, San Francisco, pp. 409-428.

4. Rabenhorst, D. W., "Composite Flywheel Development Program - Final Report", Johns Hopkins University, Applied Physics Laboratory: APL/JHU SDO-4616A NSF Grant No. AER 75-20607, May 1978.

5. Erdman, A. G., Frohrib, D. A., Garrard, W. L., Hagen, D. L., Carlson, T. P., "The Development of a Cellulose Flywheel System for Rural Wind Energy Storage: Final Report", University of Minnesota, for the Minnesota Energy Agency, July 1978.

6. Hagen, D. L., Erdman, A. G., "Economics of Cellulosic Rotors", University of Minnesota, Final Report to Johns Hopkins University, Applied Physics Laboratory, May 1979.

7. Erdman, A. G., Frohrib, D. A., Garrard, W. L., Hagen, D. L., Carlson, T. P., "The Development of a Cellulosic Flywheel System for Rural Wind Energy Storage: Phase II, A Final Report", University of Minnesota, for the Minnesota Energy Agency, December 1979.

8. McGuire, D. P. and Rabenhorst, D. W., "Composite Flywheel Rotor/Hub Attachment Through Elastomeric Interlayers:, Proc. 1977 Flywheel Technology Symposium, DOE 1978.

9. Milner, A., Lincoln Laboratory, Massachusetts Institute of Technology, Lexington, MA, private communication, 1979.

10. Gougeon Brothers, Inc., Bay City, MI, "Wooden Blade Feasibility Study, Final Progress Report", November 1978 to NASA-Lewis Research Center, Cleveland, OH.

11. Kubokawa, C. C., "Viscoelastic Foam Cushion" NASA Tech. Brief ARC-11089 & Technical Support Package. December 1976, "TEMPER FOAM" Manufactured by Edmont-Wilson, Coshocton, Ohio.

12. Eusepi, M. W., Mechanical Technology Inc., "The Application of Fluid Film Bearings and a Passive Magnetic Suspension to Energy Storage Flywheels", Proc. 1978 Mechanical and Magnetic Energy Storage Contractors Review Meeting, Luray, VA, October 1978.

13. Hagen, D. L., Erdman, A. G., Frohrib, D. A., "Design of Flywheel Rotors Utilizing Cellulosic Materials:, Paper No. 799080, 14th Intersociety Energy Conversion Engineering Conference, August 6, 1979, Boston, MA.

14. Carlson, T., "Critical Speeds of a Flywheel Energy Storage System", M.S. Plan B Paper, Mechanical Engineering Department, University of Minnesota, August 3, 1978.

15. Bert, C. W. and Chen, T. C. L., "Lateral and Tilt Whirl Modes of Flexible Mounted Flywheel Systems", Sandia Report SAND-78-7070, December 1978.

16. Bucciarelli, L., Jr., Massachusetts Institute of Technology, Cambridge, MA, private communication, August 24, 1979.

17. Wilson, T. R. C., "Strength-Moisture Relations for Wood", Technical Bulletin, No. 282, March 1932, Forest Products Lab., Forest Services, USDA.

18. Lenderink, Tom, Lenderink Inc., Belmont, MI 49306.

19. Lake Elmo Hardwood Lumber Inc., Lake Elmo, St. Paul, MN 55042

20. Plywood and Door Manufacturers Company, Inc., 1430 E. 130th Street, Lake Calumet Harbor, Chicago, IL 60633, Attn. Jervis Lang.

21. Kollman, F. P. and Cote, W. A., Jr., Principles of Wood Science and Technology, Vol. 1, Solid Wood, Springer Verlag, 1968, p. 326.

22. Mikhal 'Chenko, T. A., "Regulation of the Elastic Properties of Plywood", Lesnoi Zhurnal 1974, Vol. 17, No. 3, pp. 87-92, Russian six references.

23. Ivanov, Iu. M., "The Limit of Plastic Flow of Wood", USDA Forest Products Lab., Translation No. 111 by H. P. Kipp, August 1955.

24. Sugiyama, Hideo, "On the Effect of the Loading Time on the Strength Properties of Wood: A Review of Japanese Research", Wood Science and Technology, Vol. 1, pp. 283-303, 1967.

25. DeBaise, G. R., Porter, A. W. and Pentoney, R. E., "Morphology and Mechanics of Wood Fracture", Materials Research and Standards, Vol. 6, No. 10, pp. 493-499, October 1966.

26. Wood, W. E. and Dilipkumar, D., "Acoustic Emission Analysis of Finger Joints: A Feasibility Study", Oregon Graduate Center, Beaverton, OR, September 27, 1977.

27. Wood, W. E. and Dilipkumar, D., "A Composite Grip Design for Eliminating of Extraneous Noise During Acoustic Emission Testing", J. Test. Eval., Vol. 6, No. 6, 1978, pp. 369-370.

28. Lewis, Wayne C., "Fatigue of Wood and Glued Joints Used in Laminated Construction", Forest Prod. Res. Soc., Vol. 5, pp. 221-229, 1951.

29. Egner, K. and Rothnund, A., "Zusammenfassender Bericht über Dauerzugversuche mit Hölzern", Materialprufungsanstalt Tech. Hochschule Stuttgart, 1944.

30. Barrett, J. D. and Foschi, R. O., "Duration of Load and Probability of Failure in Wood, Part I, Modelling Creep Rupture, Part II, Constant, Ramp and Cyclic Loadings:, Canadian J. Civil Eng., Vol. 5, No. 4, 1978, pp. 505-532.

31. Gerhards, C.C., "Time Related Effects of Loading on Wood Strength: A Linear Cumulative Damage Theory", Wood Science, Vol. 11, No. 3, Jan. 1979, pp. 139-144.

32. Lazan, B. J., "Dynamic Creep and Rupture Properties of Temperature Resistant Materials under Tensile Fatigue Stress", Am. Soc. Test Materials, Vol. 49, 1949, pp. 757-787.

33. Barck, T. A., Chase, T. R., Effrem, P. C., Hartley, S. W., Nelson, E. W., Ost, R. A., Walt, M. J., "Flywheel-CVT Test Bed", Design Center Project Report, University of Minnesota, December 5, 1978.

34. Siau, J. F., Flow in Wood, Syracuse Wood Science Series, 1, Syracuse University Press, 1971.

35. Wengert, E. M., "Some Considerations in Modeling and Measuring Moisture Flow in Wood", Wood Science, Vol. 10, No. 1, July 1977, pp. 49-52.

APPENDIX

CORRECTED FATIGUE TESTER LOADINGS

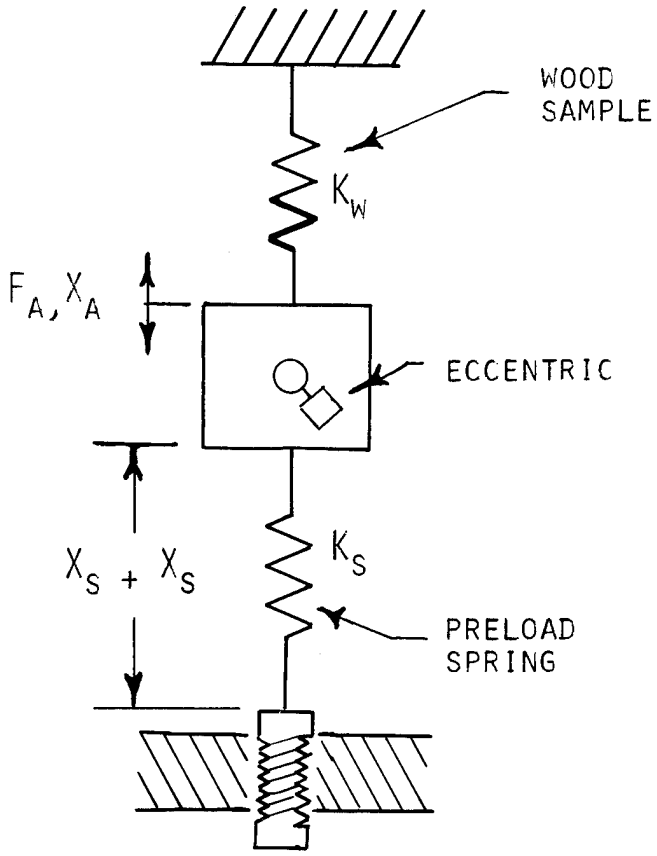

K_W - effective spring constant of wood sample lbs/in

K_S - combined spring constant of preload springs lbs/in

M - mass of eccentric cage and attached fixtures

F_a - cyclic load due to eccentric

X_a - cage displacement

ΔX_S - preset constant preload spring extension

X_S - preload spring length at relaxation

F_p - preload force

F_s - force on springs

F_w - force seen by wood sample

F_{mx} - maximum sample loading

F_{av} - mean sample loading

F_{mn} - minimum sample loading

The loadings seen by the fatigue sample are dependent on the loadings and extension in the system. The following calculations initially assume no damping which will be considered later.

The maximum force on the sample is the sum of the alternating eccentric and preload forces.

$$F_{mx} = F_p + F_a \tag{1}$$

The preload spring extension is kept constant even with sample extension and creep. The minimum force on the sample including the eccentric and cage motion is

$$F_{mn} = F_p - X_a\,(K_s - K_\omega) \tag{2}$$

Subtracting (2) from (1) we have

$$F_{mx} - F_{mn} = F_p + F_a - (F_p + X_a(K_s - K_\omega)) \tag{3}$$

$$= (1-C)F_{mx}$$

where $$C = F_{mn}/F_{mx} \tag{4}$$

Rearranging (3) we have

$$X_a = \frac{(1-C)\,F_{mx} - F_a}{K_\omega - K_s} \tag{5}$$

Introducing the motion transmissibility T

where $T = X/F/K$ we have

$$X_a = T\,\{F_a/(K_s + K_\omega)\}$$

The transmissibility T is dependent on the natural frequency and the critical damping ratio as

$$T = \frac{1}{\left\{\left(1 - \left(\frac{\omega}{\omega_n}\right)^2\right)^2 + \left(2\,\xi\,\frac{\omega}{\omega_n}\right)^2\right\}^{\frac{1}{2}}}$$

where

$$\omega_n = \left(\frac{K_s + K_w}{M}\right)^{\frac{1}{2}} = \text{natural frequency}$$

ω = operating frequency = 60 HZ

ξ = critical damping ratio

equating the two equations for X_a we have

$$F_a = \left(T \frac{k_w - k_s}{(k_s + k_w)} + 1\right)^{-1} \cdot (1 - C) F_{mx}$$

$$F_p = F_{mx} - F_a$$

$$F_{av} = F_p + k_s X_a$$

$$F_{mn} = F_p + (k_s - k_a) X_a$$

$$F_{mx} = F_p + F_a$$

DISTRIBUTION:

DOE/TIC-4500-R67 UC-94b (183)

University of Minnesota (5)
Office of Research Administration
2642 University Avenue
St. Paul, MN 55114

University of Minnesota (5)
Department of Mechanical Engineering
111 Church St. SE.
Minneapolis, MN 55455
Attn: A. G. Erdman (2)
D. L. Hagen (2)
D. A. Frohrib

Lawrence Livermore Laboratory (25)
P. O. Box 808
Livermore, CA 94550
Attn: T. M. Barlow MS L-388
D. M. King MS L-388 (24)

U.S. Department of Energy (2)
Division of Energy Storage Systems
600 East St. NW.
Washington, D.C. 20585
Attn: J. H. Swisher
P. Thompson

U.S. Department of Energy (2)
Division of Distributed Solar Technology
600 East St. NW.
Washington, D.C. 20585
Attn: R. L. San Martin
P. D. Maycock

Dr. Vance Setterholm
Forest Products Laboratory
P. O. Box 5130
Madison, WI 53705

Dr. Jerome Seaman
Deputy Director
Forest Products Laboratory
P. O. Box 5130
Madison, WI 53705

Dr. Charles Gerhards (2)
Forest Products Laboratory
P. O. Box 5130
Madison, WI 53705

Tom Peters
MK Forest Products Company
P. O. Box 7808
Boise, ID 83729

Tom Arend Lenderink
Lenderink & Associates, Inc.
Belmont, MI 49306

Jervis Lang
Plywood and Door Manufacturers
1430 E. 130th Street
Lake Calumet Harbor
Chicago, IL 60633

David Rabenhorst
Applied Physics Laboratory
Johns Hopkins University
Johns Hopkins Road
Laurel, MD 20810

Roy P. Hagen
Sui Pak Villa
Jockey Club Road
Fanling, New Territories
Hong Kong

Binayak Bhadra
2810 N.W. Orchard Street
Corvalis, OR 97331

Borg Madsen
University of British Columbia
Department of Civil Engineering
Vancouver, B.C.
Canada

Dr. Frank Stark
713 Cherry
Chillicothe, MO 64601

Al Schlorholtz (2)
Acting EDB Secretary
UMN, P. O. Box 126
Kathmandu
Nepal

Kristian Kousholt
Building Materials Laboratory
Technical University of Denmark
DK 3400 Hillerød
Denmark

Dr. John Haygreen
Forest Products Department
203 Kaufert Lab
University of Minnesota
St. Paul, MN 55114

Dr. Roland D. Gertjejansen
Forest Products Department
102 Kaufert Lab
University of Minnesota
St. Paul, MN 55114

Dr. James Bowyer
Forest Products Department
204 Kaufert Lab
University of Minnesota
St. Paul, MN 55114

Dr. Andy Frank
Mechanical Engineering Department
University of Wisconsin
Madison, WI 53715

Rand Clausen
Fish Enterprises
107 4th Street S.E.
Minneapolis, MN 55414

Carol Baldwin
Tree Collection
Engineering Library, Lind Hall
University of Minnesota
Church Street S.E.
Minneapolis, MN 55455

Dr. Preben Hoffmeyer
Gl Frederiksborgvej 28
DK 3400 Hillerød
Denmark

Professor Hideo Sugiyama
Department Forest Products
Faculty of Agriculture
University of Tokyo
1-1-1 Yayoi, Bunyo-su
Tokyo, Japan

Dr. W. E. Wood
Oregon Graduate Center
Beaverton, OR 97005

Dr. L. Bucciarelli, Jr.
Massachusetts Institute of Technology
Cambridge, MA 02140

Dr. A. Milner
Lincoln Laboratory
Massachusetts Institute of Technology
Cambridge, MA 02140

Curt Dechow
Gougeon Brothers, Inc.
706 Martin Street
Bay City, MI 48706

Hans Baumen
Blomberger Holtzindustries
1579 Treetop Road
Peterborough, Ontario
Canada

J. F. Wooldridge
Market Development Manager
National Standard Company
Niles, MI 49120

Dr. F. A. Johnson
Composite Products
Weyerhauser Company WTC-1B4
Tacoma, WA 98401

Dr. R. Ramakumar
School of Electrical Engineering
202 Engineering South
Oklahoma State University
Stillwater, OK 74074

Dr. A. J. Nanany (2)
Eastern Forest Products Lab
Environment Canada
800 Montreal Road
Ottawa K1AOW5
Canada

Arthur E. Raynard
Airesearch Manufacturing Company
of California
Division of the Garrett Corporation
2525 W. 190th Street
Torrance, CA 90509

Raute, Inc.
1377 Barclay Circle
Suite 1
P. O. Box 1287
Marietta, GA 30060

Dr. J. D. Barrett (2)
Forintek Canada Corporation
Western Forest Products Laboratory
6620 N.W. Marine Drive
Vancouver, B.C.
Canada V6T 1X2

Forestry Library
Green Hall
University of Minnesota
St. Paul, MN 55414

Bob Yoder
Riley Robb Hall
Cornell University
Ithaca, NY 14853

Dott. Ing. Giancarlo Genta
Instituto Della Motorizzazione
Politecnico Di Torino
C. Duca Degli Abruzzi, 24
10129 Torino
Italy

Ebbe Lundgren
The Lund Institute of Technology
Institute of Mechanics
Fac 725
S-220 07 Lund 7
Sweden

2320 K. L. Gillespie
2324 R. S. Pinkham
2324 H. E. Schildknecht (2)
4715 R. H. Braasch
4719 D. G. Schueler
4740 R. K. Traeger
4744 H. M. Dodd
4744 B. C. Caskey
5811 L. A. Harrah
8266 E. A. Aas
3144 T. L. Werner (5)
3151 W. L. Garner (3)
For DOE/TIC (Unlimited Release)

Org.	Bldg.	Name	Rec'd by *	Org.	Bldg.	Name	Rec'd by *

* Recipient must initial on classified documents.